GFZ

Helmholtz-Zentrum
POTSDAM

HELMHOLTZ-ZENTRUM POTSDAM
DEUTSCHES
GEOFORSCHUNGSZENTRUM

I. Bergmann–Wolf, R. Dill, E. Forootan, V. Klemann,
J. Kusche, I. Sasgen, H. Dobslaw

Updating ESA's Earth System Model for Gravity Mission Simulation Studies

2. Comparison with the Original Model

Scientific Technical Report STR14/08

www.gfz-potsdam.de

HELMHOLTZ
GEMEINSCHAFT

Recommended citation:

Bergmann-Wolf, I., Dill, R., Forootan, E., Klemann, V., Kusche, J., Sasgen, I., Dobslaw, H. (2014), Updating ESA's Earth System Model for Gravity Mission Simulation Studies: 2. Comparison with the Original Model. *Scientific Technical Report 14/08, GFZ German Research Centre for Geosciences*. doi: 10.2312/GFZ.b103-14088.

Imprint

Helmholtz Centre Potsdam
GFZ German Research Centre for Geosciences

Telegrafenberg
D-14473 Potsdam

Published in Potsdam, Germany
August 2014

ISSN 1610-0956

DOI: 10.2312/GFZ.b103-14088
URN: urn:nbn:de:kobv:b103-14088

This work is published in the GFZ series
Scientific Technical Report (STR)
and electronically available at GFZ website
www.gfz-potsdam.de

ESA Contract No. 4000109421

Updating ESA's Earth System Model for Gravity Mission Simulation Studies

2. Comparison with the Original Model

Doc. No.: ESAESM_ND2_i1r2
Issue: 1
Revision: 2
Date: August 5, 2014
Authors: I. Bergmann–Wolf, R. Dill, E. Forootan, V. Klemann, J. Kusche, I. Sasgen, H. Dobslaw
ESA TO: R. Haagmans (ESTEC)

GFZ Potsdam, Department Geodesy and Remote Sensing

Scientific Technical Report STR 14/08
DOI: 10.2312/GFZ.b103-14088

ESA Study Contract Report

ESA Contract No.	Subject		Contractor
4000109421	Updating ESA's Earth System Model for Gravity Mission Simulation Studies		GFZ German Research Centre for Geosciences
ESA CR No.	**STAR CODE**	**No. of Volumes:** 3 **This is Volume No.** 2	**Contractors Reference**

Abstract

The ability of any satellite gravity mission concept to monitor mass transport processes in the Earth system is typically tested well ahead of its implementation by means of various simulation studies. Those studies often extend from the simulation of realistic orbits and instrumental data all the way down to the retrieval of global gravity field solution time-series. Basic requirement for all these simulations are realistic representations of the spatio-temporal mass variability in the different sub-systems of the Earth, as a source model for the orbit computations.

For such simulations, a suitable source model is required to represent (i) high-frequency (i.e., sub-daily to weekly) mass variability in the atmosphere and oceans, in order to realistically include the effects of temporal aliasing due to non-tidal high-frequency mass variability into the retrieved gravity fields. In parallel, (ii) low-frequency (i.e., monthly to interannual) variability needs to be modelled with realistic amplitudes, particularly at small spatial scales, in order to assess to what extent a new mission concept might provide further insight into physical processes currently not observable.

The new source model documented here attempts to fulfil both requirements: Based on ECMWF's recent atmospheric reanalysis ERA-Interim and corresponding simulations from numerical models of the other Earth system components, it offers spherical harmonic coefficients of the time-variable global gravity field due to mass variability in atmosphere, oceans, the terrestrial hydrosphere including the ice-sheets and glaciers, as well as the solid Earth. Simulated features range from sub-daily to multiyear periods with a spatial resolution of spherical harmonics degree and order 180 over a period of 12 years. In addition to the source model, a de-aliasing model for atmospheric and oceanic high-frequency variability with augmented systematic and random noise is required for a realistic simulation of the gravity field retrieval process, whose necessary error characteristics are discussed.

The documentation is organized as follows: The characteristics of the updated ESM along with some basic validation are presented in Volume 1 of this report (Dobslaw *et al.*, 2014). A detailed comparison to the original ESA ESM (Gruber *et al.*, 2011) is provided in Volume 2 (Bergmann-Wolf *et al.*, 2014), while Volume 3 (Forootan *et al.*, 2014) contains a description of the strategy to derive a realistically noisy de-aliasing model for the high-frequency mass variability in atmosphere and oceans.

The files of the updated ESA Earth System Model for gravity mission simulation studies are accessible at DOI:10.5880/GFZ.1.3.2014.001.

Authors:

I. Bergmann–Wolf, R. Dill, E. Forootan, V. Klemann, J. Kusche, I. Sasgen, H. Dobslaw

Name of ESA Study Manager	ESA Budget Heading
Roger Haagmans Section: Earth Surfaces and Interior Section Division: Mission Science Division Department: Science, Application and Future Technologies	

Scientific Technical Report STR 14/08
DOI: 10.2312/GFZ.b103-14088

Contents

List of Figures

Scientific Technical Report STR 14/08
DOI: 10.2312/GFZ.b103-14088

Chapter 1

Introduction

The realistic assessment of candidate constellations for a future satellite gravity mission dedicated to the observation of large-scale mass transport phenomena requires extensive end-to-end simulations: starting from simulated orbits based on a realistic global model of large-scale mass redistributions that cause time-changes in the gravity field all the way down to the retrieval of global gravity field solutions and the application of appropriate post-processing techniques to remove spatially anisotropic errors. A critically important prerequisite for such simulations is a model of the time-variable gravity field of the Earth that contains realistic variability on a wide range of spatial and temporal scales important for satellite gravimetry.

Within this volume, we present a detailed comparison of the characteristics of the updated ESA Earth System Model (updated ESM) with the original version of Gruber *et al.* (2011). After some general recommendations for the replacement of the original with the updated model in satellite simulation set-ups (Chapter 2), we show comparisons separately for the individual components A (Chapter 3), AO (Chapter 4), O (Chapter 5), H (Chapter 6), I (Chapter 7), S (Chapter 8), and AOHIS (Chapter 9). In the final Chapter 10, a comparison of the sub-diurnal signal contained in atmosphere and ocean is discussed.

Chapter 2

Guidelines for Replacement

Many conventions applied in the original ESA ESM have not been altered in the updated version. The most important changes besides the application of new geophysical data-sets are summarized in this chapter together with suggestions on how to transform the original or the updated ESM to make both data-sets comparable, and thus allow for an easier replacement of the original model with the update in a satellite gravity mission simulation environment.

2.1 Reference Epoch

Time variations in the gravity field are typically described as anomalies $\Delta V(\lambda, \varphi, t)$ with respect to a certain reference field $V_0(\lambda, \varphi, t)$:

$$\Delta V(\lambda, \varphi, t) = V(\lambda, \varphi, t) - V_0(\lambda, \varphi, t) \tag{2.1}$$

The choice of the reference field is somewhat arbitrary, in the case of the GRACE gravity fields, usually a static gravity field serves as the reference field, which implicitly refers to a certain period in time related to the observations included. For the calculation of the time-variable background model GRACE AOD1B RL05, a time-averaged field over the years 2001 and 2002 is used.

For the original ESA ESM (Gruber *et al.*, 2011), the individual reference field for every component A, O, H, I, and S has been chosen to be the first data-set of the model period, i.e., Jan 1st 1995, 00:00 UTC. For this epoch, ΔV is identically zero at every position for every component.

For the updated ESM, the individual reference field for every component A, O, H, I, and S has been chosen to be the time-average over all 6 hourly time-steps of the years 1995 - 2006.

To transform a component of the updated ESM to the reference epoch used by Gruber et al. (2011), subtract the set of coefficients of the first data-set of the model period, i.e., Jan 1st, 1995, 00:00 UTC from every data-set of the whole time-series.

To transform a component of the original ESA ESM to the reference epoch used in the update, calculate the time-average over all time-steps of the years 1995 -2006, and subtract this set of coefficients from every data-set of the whole time-series.

2.2 Modified IB-Correction

The oceanic component of the updated ESM is inverse-barometrically (IB) corrected, and the atmospheric component is consequently modified as well in order to keep the sum of A and O

unaffected. The component A of the original ESA ESM is thus only comparable to the component AnoIB of the updated ESM. However, since the IB-correction does not change the ocean bottom pressure as the sum of the overlying atmospheric and oceanic masses, the sum of A+O of both ESM versions is directly comparable again. An non-IB ocean component of the updated ESM might be constructed by adding the difference of the components AnoIB and A to the O component.

2.3 Tidal Components

The atmospheric semi-diurnal tide $S_2(p)$ has a Nyquist period of 6 hours. It is thus partially aliased in a data-set with 6 hourly sampling into a standing wave pattern. To avoid those aliasing artifacts, the $S_2(p)$ signals in the atmosphere and their corresponding oceanic response have been estimated and removed from the updated ESM.

To transform a component of the original ESA ESM, estimate and subtract the tidal signal at (00:00 and 12:00) and (06:00 and 18:00) UTC, respectively. To transform a component of the updated model, estimate the tidal signal at (00:00 and 12:00) and (06:00 and 18:00) UTC, respectively from the corresponding component of the original ESA ESM, and add it to the updated version.

Chapter 3

Atmospheric Mass Variability Without IB-Correction

3.1 Global Low-Degree Coefficients

Since the original ESA ESM does not include a modified IB-correction for its atmospheric component, the original model is compared here against the component AnoIB of the updated ESM. Time-series of low-degree spherical harmonic coefficients are given in Fig. 3.1. We note in general good correspondence, in particular with respect to linear trends and sesasonal variability. A shift in total atmospheric mass in the original ESA ESM is related to the transition between ERA-40 (1995 - 2000) and the operational ECMWF analyses (2001 - 2006). Offsets between the original and the updated coefficients are related to the choice of the reference epoch: whereas the original ESA ESM arbitrarily uses the mass anomalies at Jan 1st, 1995 as the reference, the updated ESM is centered gridpoint-wise around zero. Consequently, also the low-degree coefficients are centered around zero, whereas the original model is shifted away from it.

In addition, we also present low-degree coefficients for the A component of the updated ESM under the modified IB-correction (Fig. 3.2). Total atmospheric mass and therefore C_{00} is not affected by the IB-correction and remains identical to AnoIB. Other components show substantially less variability, since signals over the oceanic regions are largely reduced by applying the IB-correction. We will provide more arguments for the use of IB-corrected ESM model components during the discussion of the ocean component in Chapter 5.

3.2 Spatial Patterns of Trends and Variabilities

The pattern of linear trends in the original ESA ESM is dominated by small-scale features over the continents. Differences in the orographies applied in ERA-40 and the operational analyses cause jumps in atmospheric surface pressure on Jan 1st, 2001 which map into the empirically derived trends with rates of more than 1 hPa a^{-1} (Fig. 3.3). Although such jumps might be rectified a posteriori by means of an appropriate post-processing procedure, it is easier to avoid such issues at all by applying a more homogeneous atmospheric data-set as in the updated ESM. Here, trends over the continents are substantially smaller and rather large-scale, which can be related to low-frequency climate variability rather than to technical issues.

For the variability of de-trended daily means, we note comparable signals for both versions of ESA ESM (Fig. 3.4). Similar conclusions are also drawn for the low-frequency part of the variability

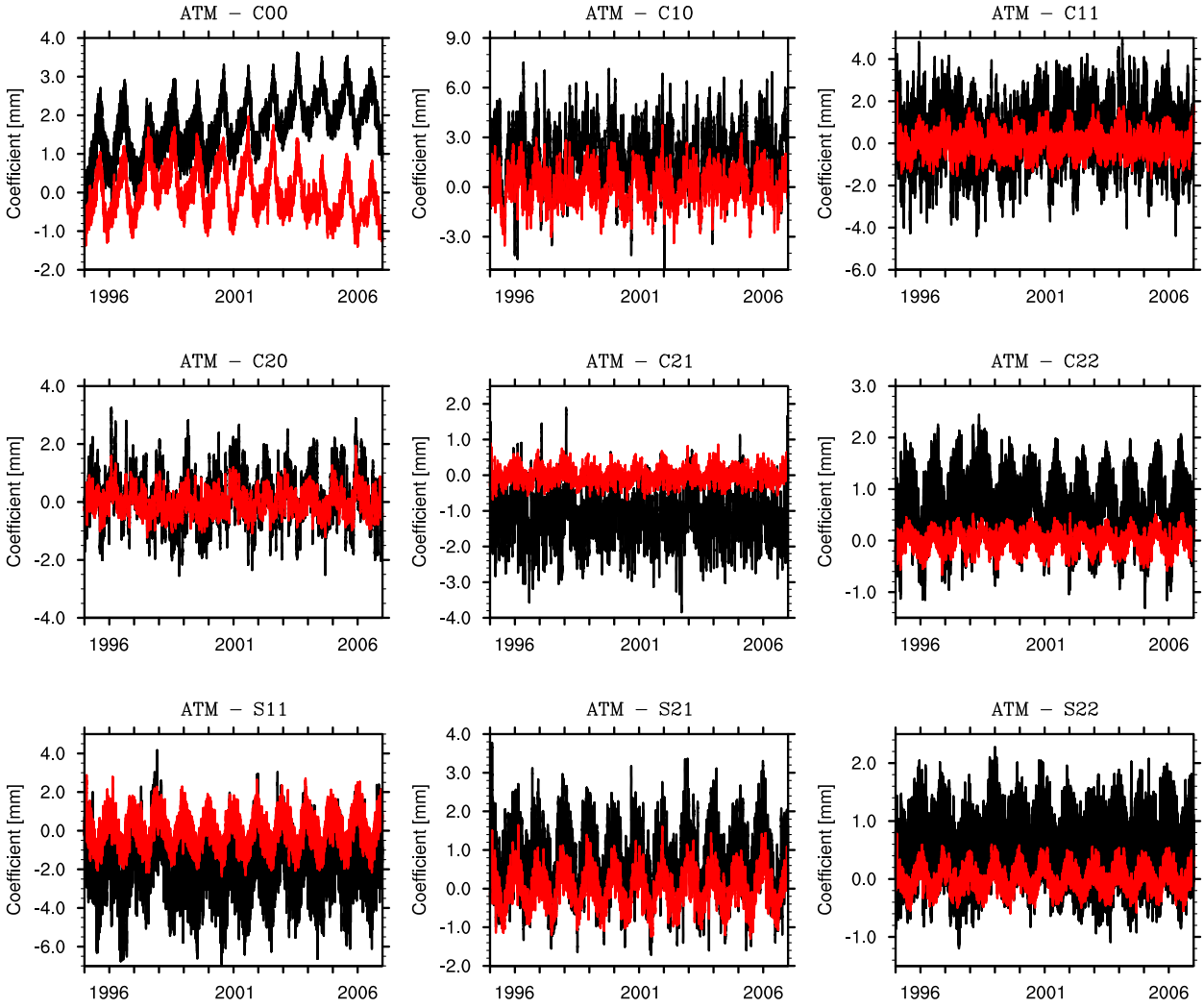

Figure 3.1: Time series (1995-2006) of low degree spherical harmonic coefficients of atmospheric surface pressure anomaly (IB-correctedi A component). The coefficients from the original ESM are shown in black, that from the updated ESM in red.

spectrum at periods longer than 30 days (Fig. 3.5). When calculating those variability plots individually for all 12 years of both ESA ESM versions (Fig. 3.7) we note some year-to-year changes which are well in the range of natural climate variability, but sufficiently close to each other to conclude that the atmospheric component of ESA ESM is sufficiently stationary to compare satellite mission simulation results from different years with each other.

For the high-frequency part of the spectrum at periods between 1 and 30 days (Fig. 3.6), both versions largely agree. When calculating those variability plots individually for all 12 years of both ESA ESM versions (Fig. 3.8), we note some year-to-year changes as before, but no apparently artificial jumps or shifts in the variability level.

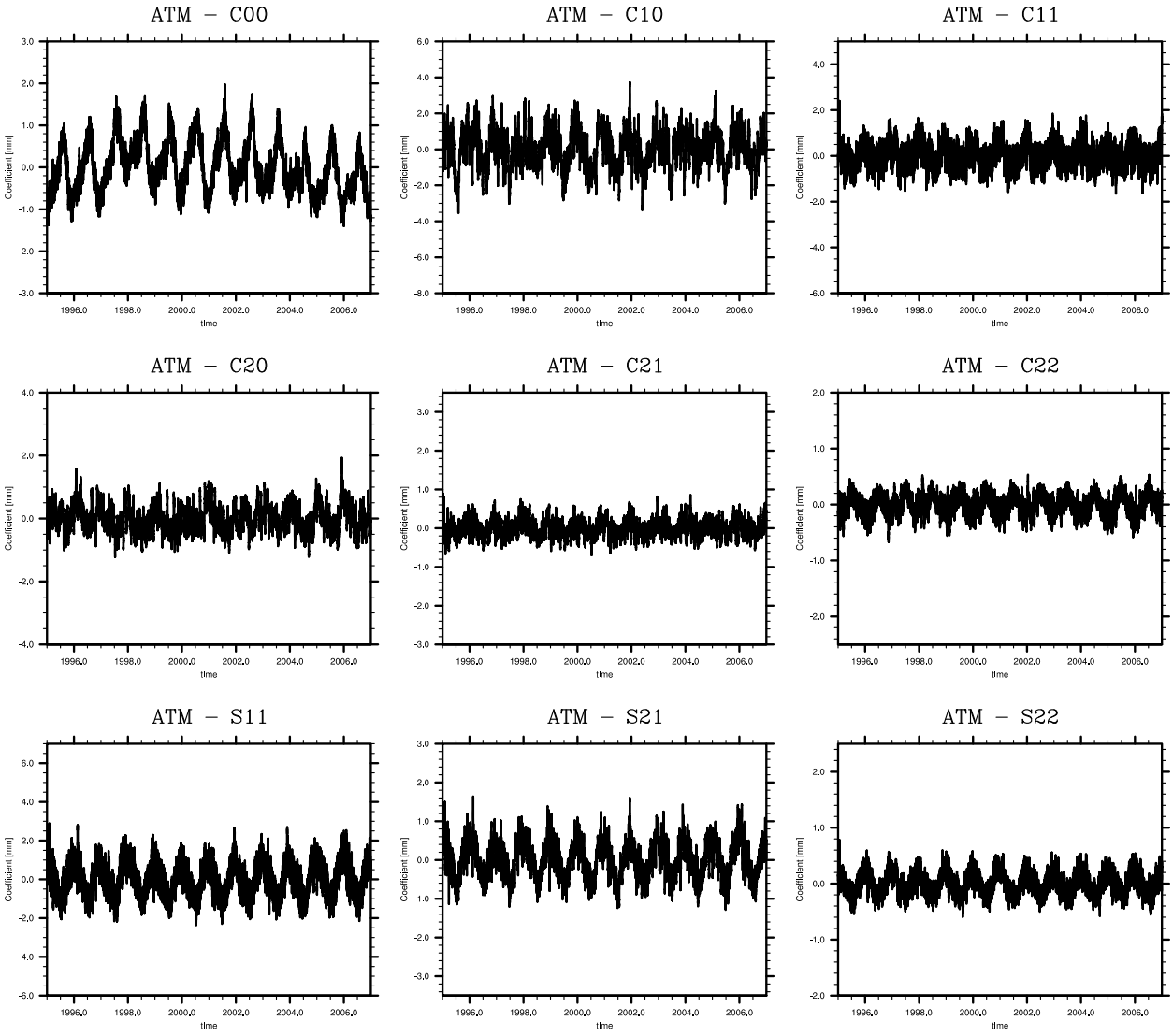

Figure 3.2: Time series (1995-2006) of low degree spherical harmonic coefficients of atmospheric surface pressure anomaly (IB-corrected A component) from the updated ESM.

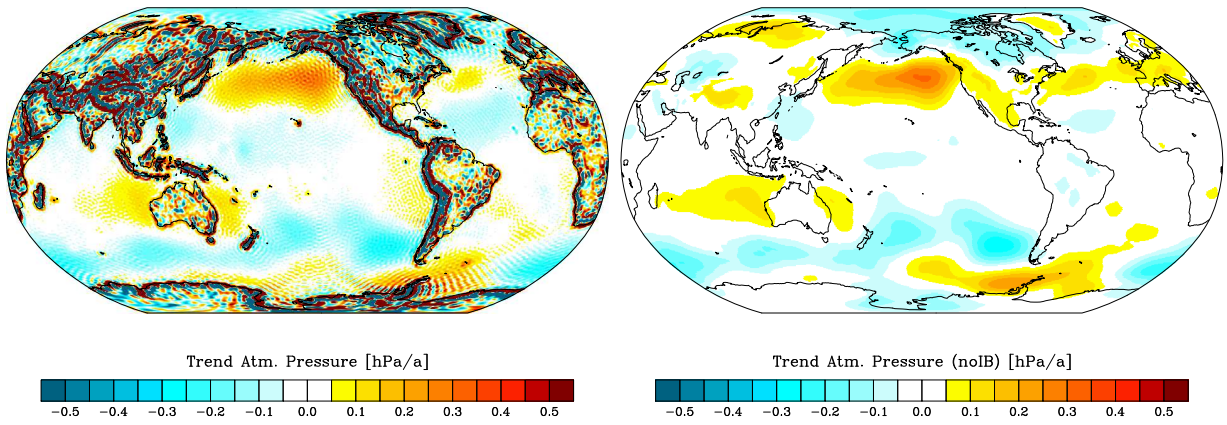

Figure 3.3: Local secular trends (1995-2006) at 0.5° spatial resolution obtained from the re-synthesized coefficients of the AnoIB component from the original (left) and updated ESM (right).

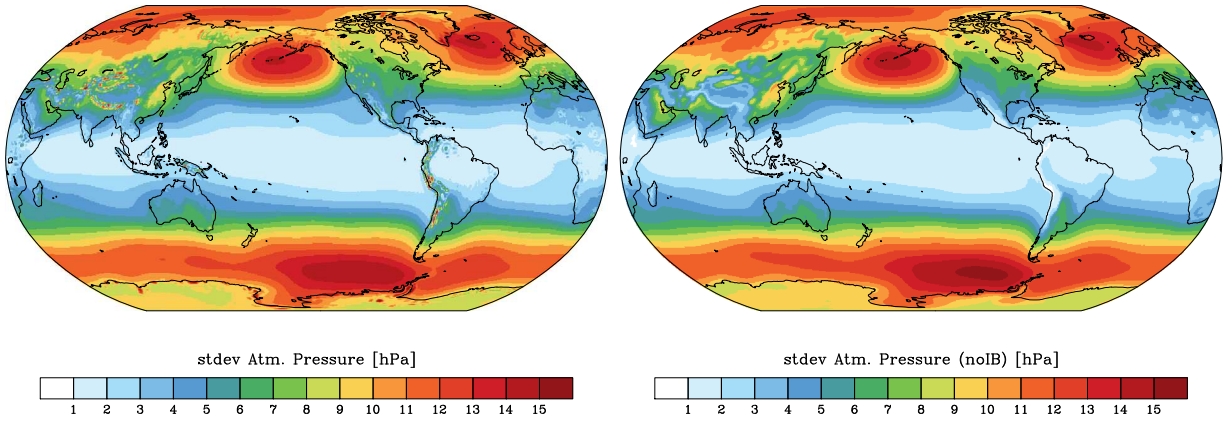

Figure 3.4: Standard deviation of atmospheric surface pressure anomaly (non-IB) (1995-2006) at 0.5° spatial resolution obtained from the re-synthesized and locally detrended coefficients of the AnoIB component from the original (left) and updated ESM (right).

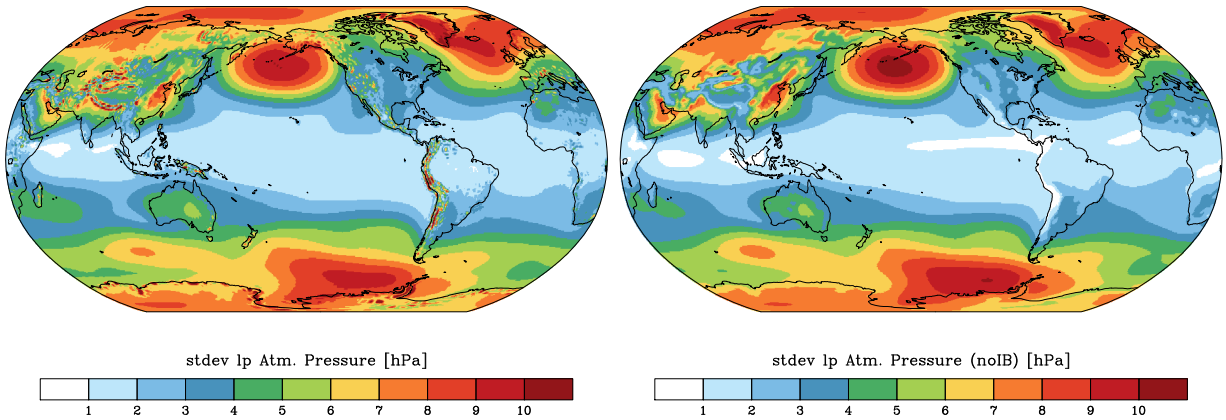

Figure 3.5: Standard deviation of atmospheric surface pressure anomaly (non-IB) (1995-2006) at 0.5° spatial resolution obtained from the re-synthesized, locally detrended and low-pass filtered (30 day cut-off) coefficients of the AnoIB component from the original (left) and updated ESM (right).

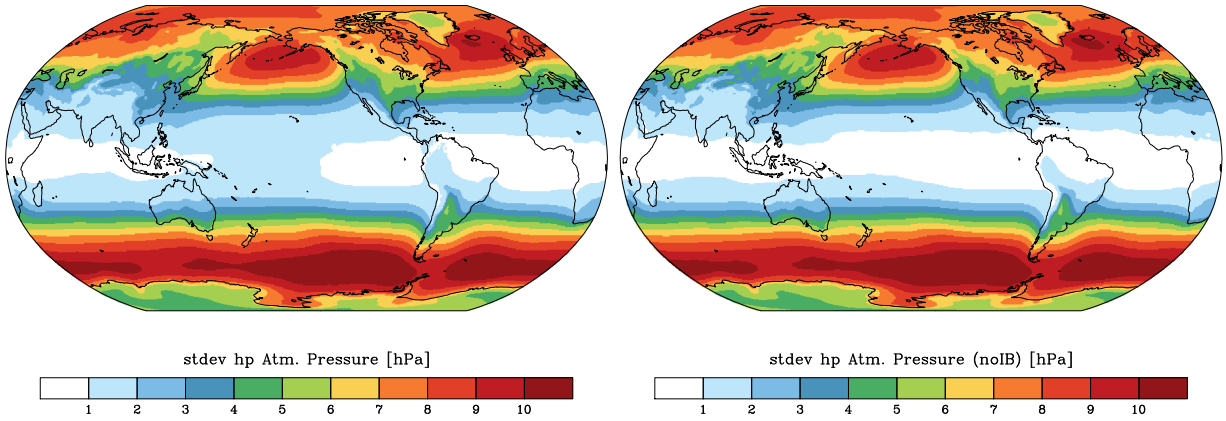

Figure 3.6: Standard deviation of atmospheric surface pressure anomaly (non-IB) (1995-2006) at 0.5° spatial resolution obtained from the re-synthesized, locally detrended and high-pass filtered (30 day cut-off) coefficients of the AnoIB component from the original (left) and updated ESM (right).

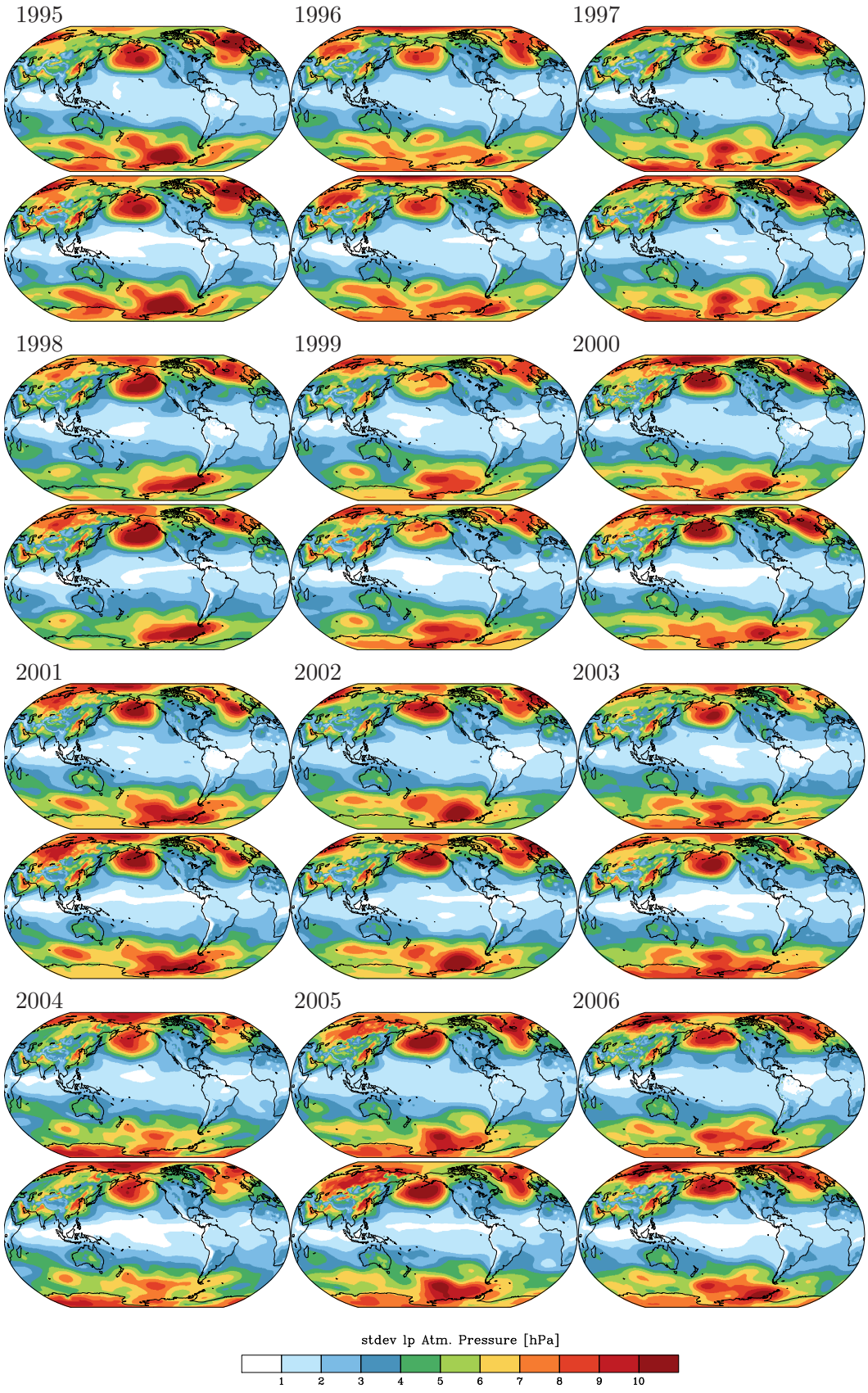

Figure 3.7: Standard deviation of atmospheric surface pressure anomaly (non-IB) at 0.5° spatial resolution obtained from the re-synthesized, locally detrended and low-pass filtered (30 day cut-off) coefficients of the AnoIB component from original (first) and updated ESM (second row) for each year between 1995 and 2006.

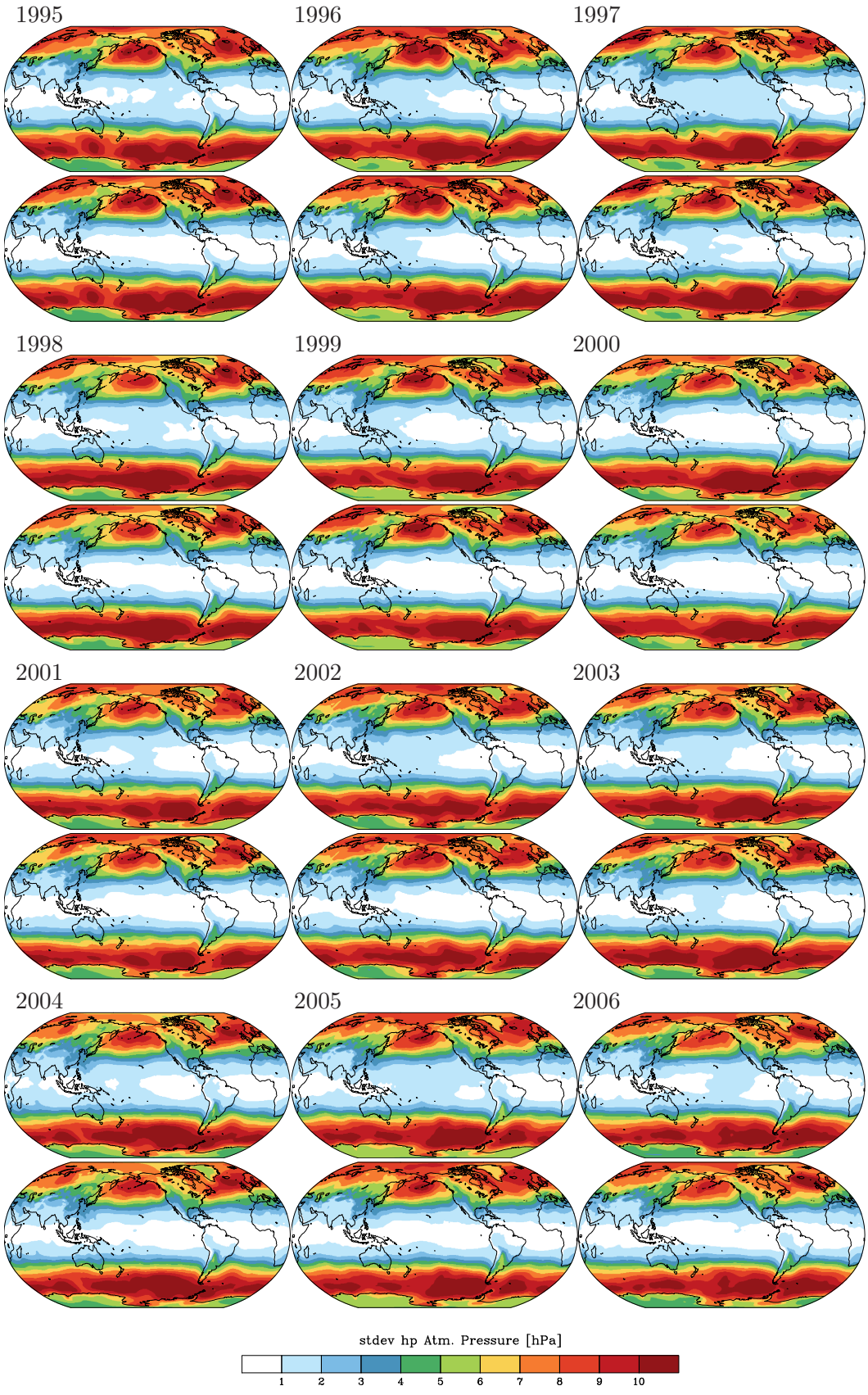

Figure 3.8: Standard deviation of atmospheric surface pressure anomaly (non-IB) at 0.5° spatial resolution obtained from the re-synthesized, locally detrended and high-pass filtered (30 day cut-off) coefficients of the AnoIB component from original (first) and updated ESM (second row) for each year between 1995 and 2006.

Chapter 4

Combined Atmosphere and Ocean Variability

4.1 Global Low-Degree Coefficients

We are going to compare here the sum of the A and O components of the updated ESM which have been processed both under the modified IB-correction with the sum of the A and O components of the original ESA ESM (Fig. 4.1). C_{00} reflects here the sum of atmospheric and oceanic total mass variations that is dominated by the eustatic sea-level variability. For the years 1995 - 2005, both ESA ESM versions agree with each other within certain limits, even though the updated ESM does show a more regular seasonal cycle in global eustatic sea-level variability that is more in line with observations. For the year 2006, the original ESA ESM exhibits a steep increase in total ocean mass, which is clearly artificial. All other low-degree coefficients have plausible variability in both model versions.

4.2 Spatial Patterns of Trends and Variabilities

Trend pattern are dominated once more by the effect of the jump on Jan 1st, 2001 (Fig. 4.2). Over the oceans, we note rather strong positive trends also in the Arctic ocean, where almost no signal is visible in the update. In addition, spatial leakage from land to the oceans is more severe in the original version due to the much stronger continental trend signals.

Variability of the de-trended daily means is fairly equal for both versions (Fig. 4.3), but we note, however, signals at much smaller scales in the updated ESM thanks to the inclusion of high-resolution information from the MPIOM STORM model run. Similar conclusions can be also drawn for the low-frequency part of the spectrum (Fig. 4.4). An analysis of the variability for the individual years (Fig. 4.6) does not reveal anomalous signals in any particular year.

For the high-frequency part of the spectrum, we also note a generally good correspondence between both ESA ESM versions (Fig. 4.5), and also the yearly analysis does not indicate any problems in a particular year (Fig. 4.7).

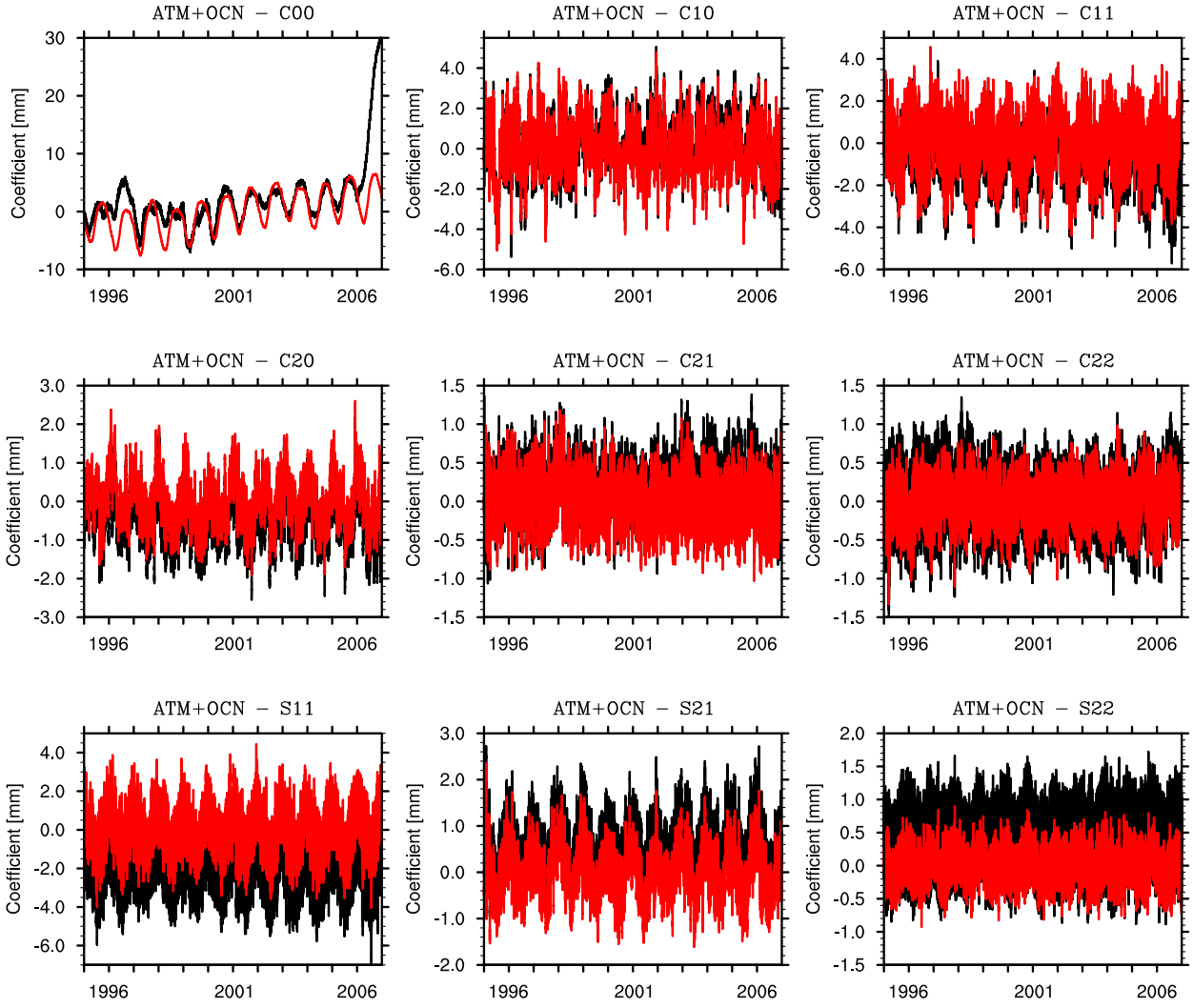

Figure 4.1: Time series (1995-2006) of low degree spherical harmonic coefficients of atmospheric surface and ocean-bottom pressure anomaly (AO component). The coefficients from the original ESM are shown in black, that from the updated ESM in red.

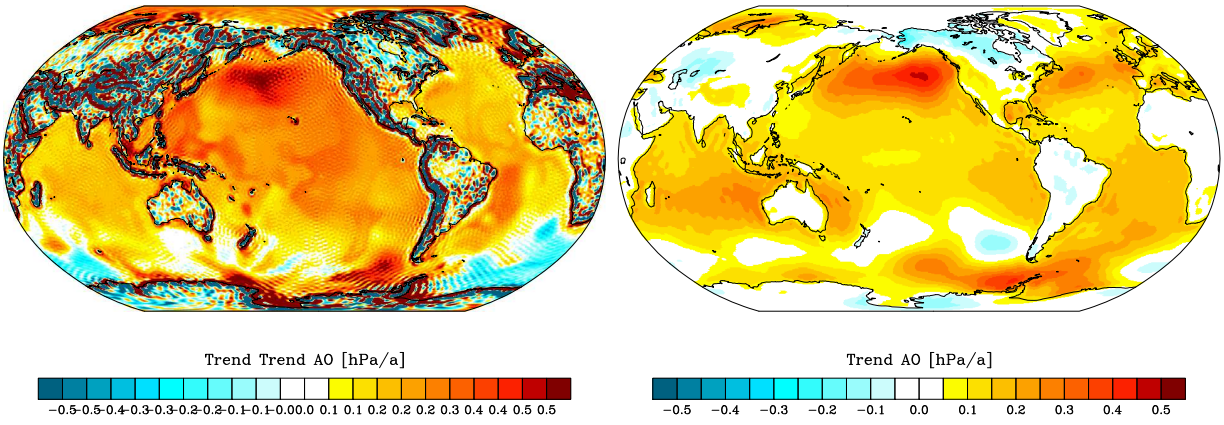

Figure 4.2: Local secular trends (1995-2006) at 0.5° spatial resolution obtained from the re-synthesized coefficients of the AO component from the original (left) and updated ESM (right).

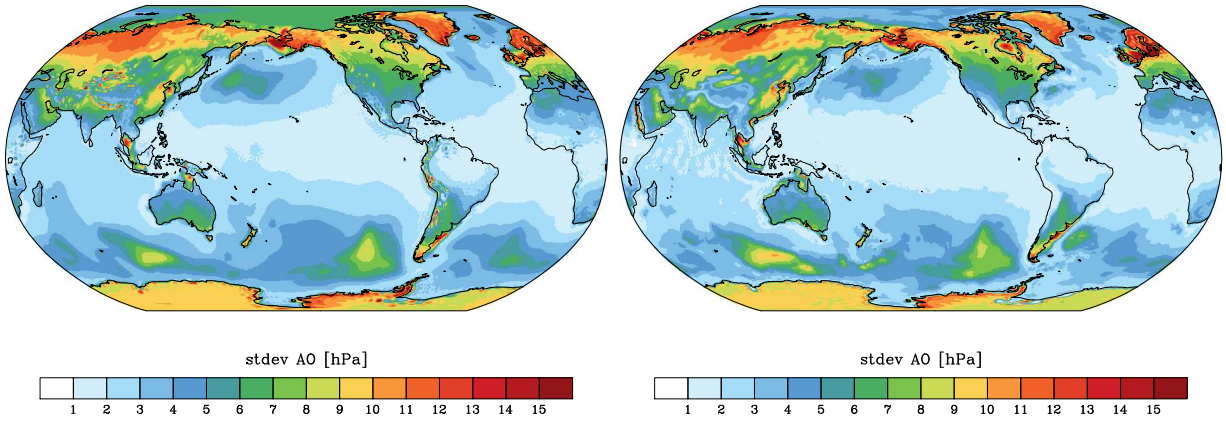

Figure 4.3: Standard deviation of atmospheric surface and ocean-bottom pressure anomaly (1995-2006) at 0.5° spatial resolution obtained from the re-synthesized and locally detrended coefficients of the AO component from the original (left) and updated ESM (right).

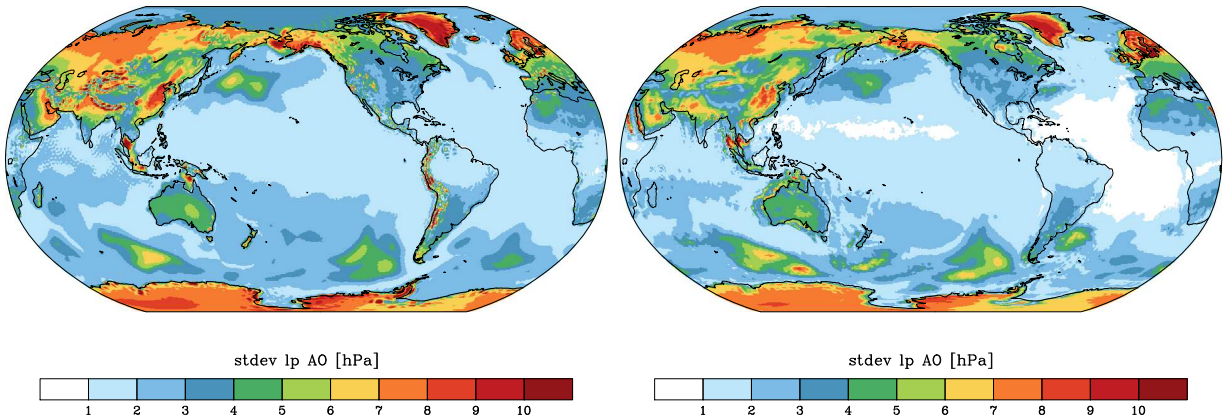

Figure 4.4: Standard deviation of atmospheric surface and ocean-bottom pressure anomaly (1995-2006) at 0.5° spatial resolution obtained from the re-synthesized, locally detrended and low-pass filtered (30 day cut-off) coefficients of the AO component from the original (left) and updated ESM (right).

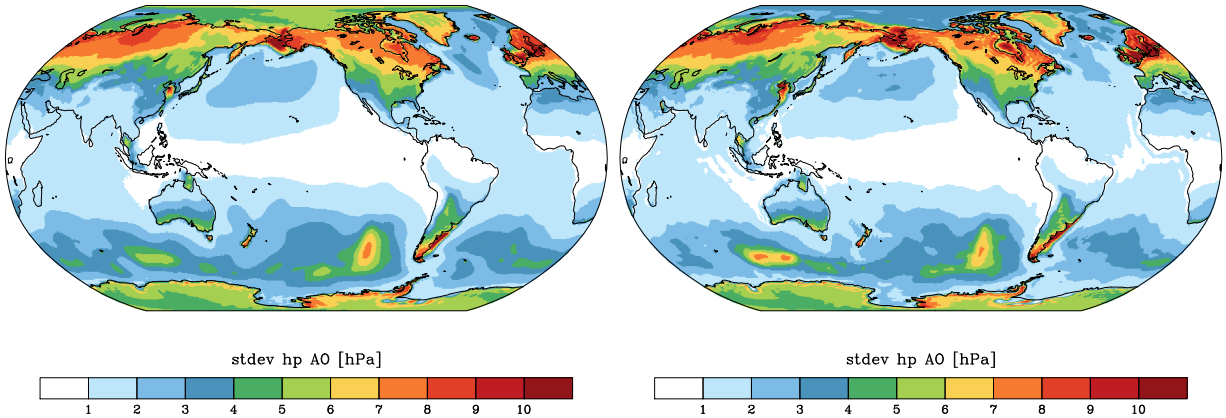

Figure 4.5: Standard deviation of atmospheric surface and ocean-bottom pressure anomaly (1995-2006) at 0.5° spatial resolution obtained from the re-synthesized, locally detrended and high-pass filtered (30 day cut-off) coefficients of the AO component from the original (left) and updated ESM (right).

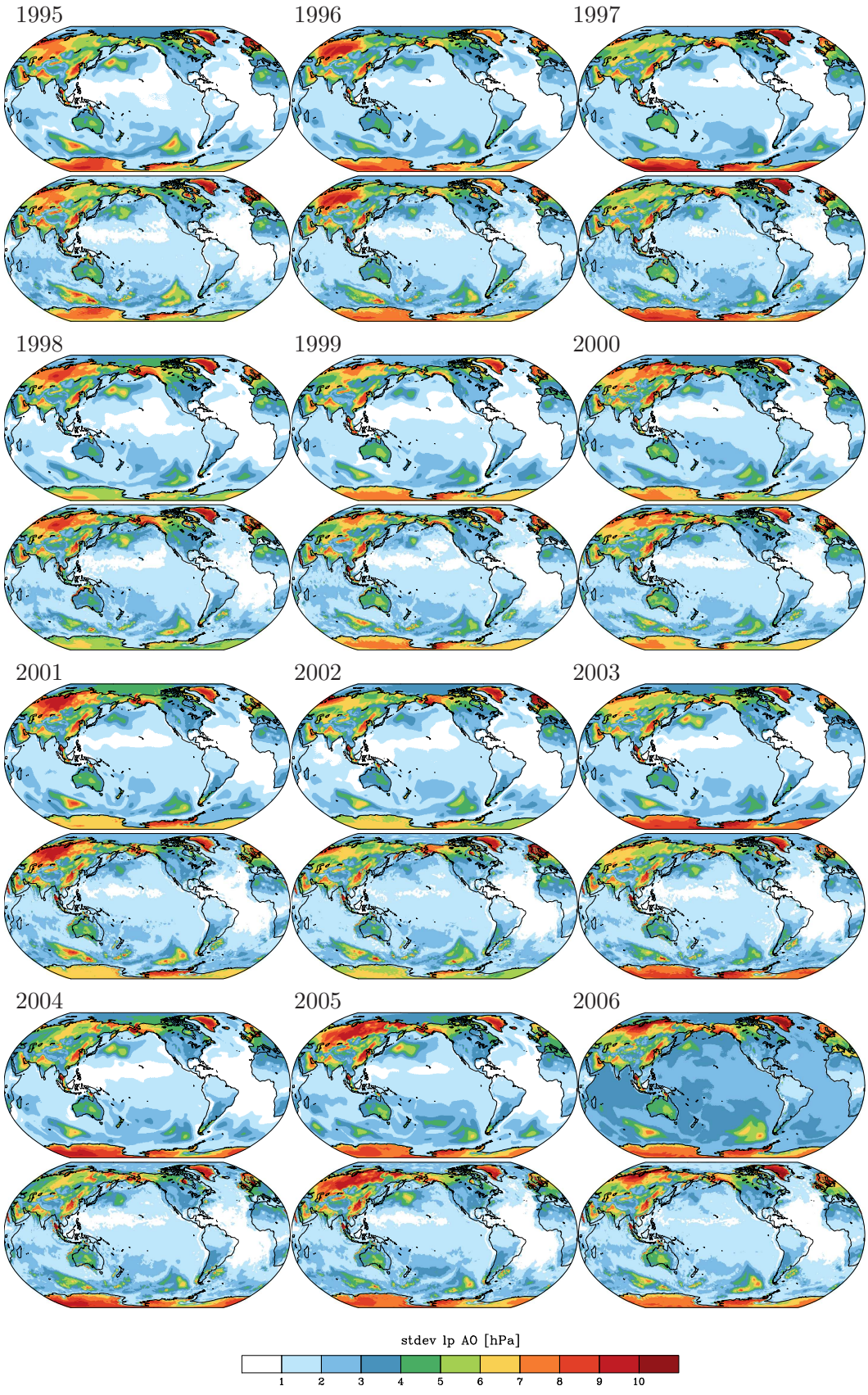

Figure 4.6: Standard deviation of atmospheric surface and ocean-bottom pressure anomaly at 0.5° spatial resolution obtained from the re-synthesized, locally detrended and low-pass filtered (30 day cut-off) coefficients of the AO component from original (first) and updated ESM (second row) for each year between 1995 and 2006.

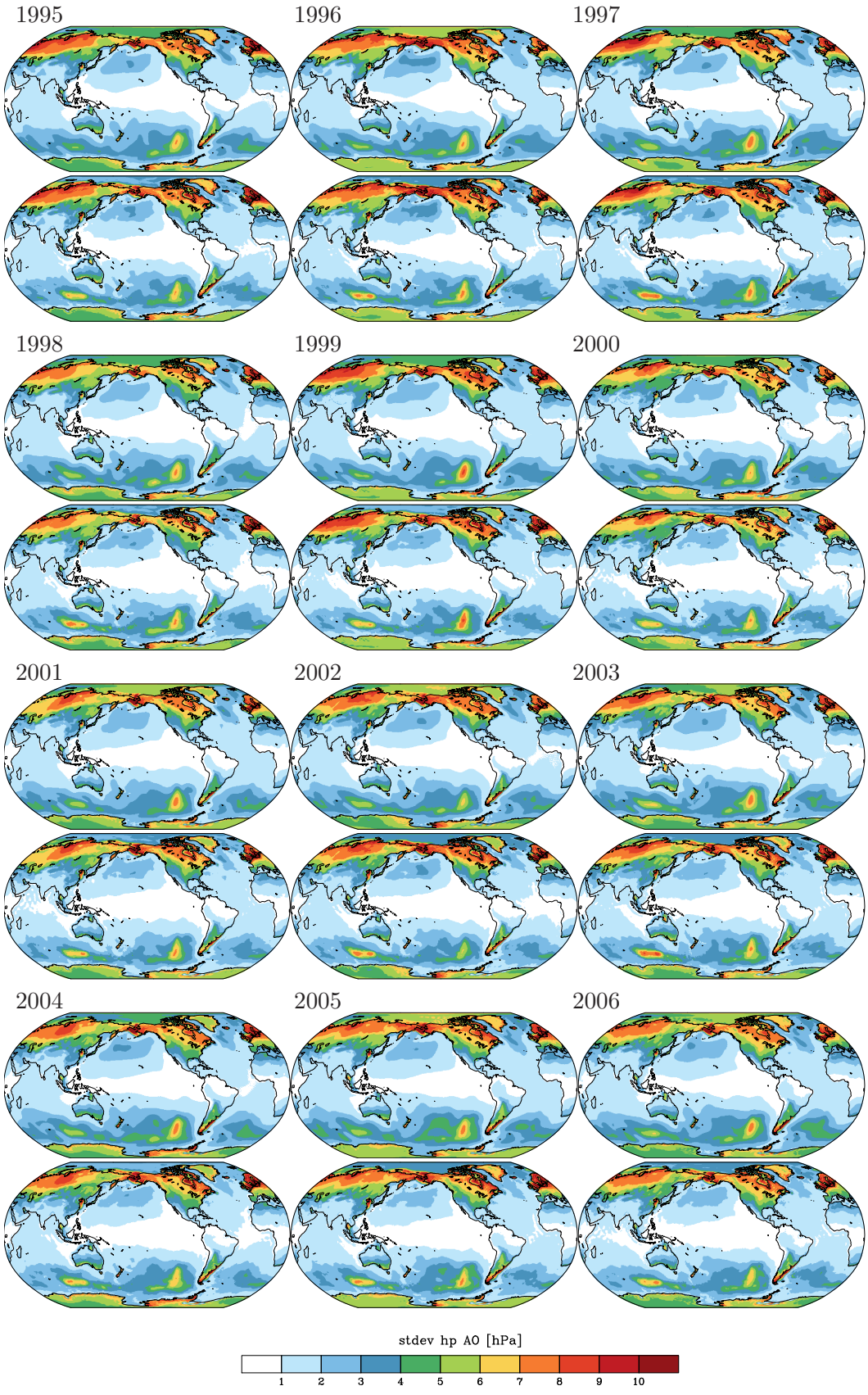

Figure 4.7: Standard deviation of atmospheric surface and ocean-bottom pressure anomaly at 0.5° spatial resolution obtained from the re-synthesized, locally detrended and high-pass filtered (30 day cut-off) coefficients of the AO component from original (first) and updated ESM (second row) for each year between 1995 and 2006.

Chapter 5

Sea-Water Contribution to Ocean Bottom Pressure

5.1 Global Low-Degree Coefficients

The oceanic components of the original and the updated ESM are not directly comparable, since the modified IB-correction is applied to the component O of the updated ESM. We nevertheless contrast both versions in order to demonstrate that the application of the modified IB-correction indeed contributes greatly to the interpretability of the oceanic component when viewed in isolation.

Low-degree coefficients (Fig. 5.1) of d = 0 reflect global eustatic ocean mass variations, where once more the erroneous increase in eustatic sea-level during 2006 in the original ESA ESM is visible. In addition, a markedly reduced variability is apparent in particular for the C_{2x} terms. Since variability of those terms is similarly high for the sum of A and O as discussed in the previous chapter, this underlines the fact that the strong anti-correlations between the A and O component are largely removed under the modified IB-correction. This is important, since only uncorrelated contributors to the time-variable gravity field may be treated as independent variables in subsequent performance analyses of satellite mission candidate concepts.

5.2 Spatial Patterns of Trends and Variabilities

Trend pattern of the oceanic component of the original ESA ESM are slightly more patchy than the updated version, and partly reflect additive-inversly the trends seen in the atmospheric masses over oceanic regions (Fig. 5.3). The reason for the trend signals visible over land are currently unknown, but the pattern suggest an effect of very low degree of the spherical harmonic expansion here; presumably, it is a degree-1 signal.

Low-frequency variability in the oceanic component of the original ESA ESM is dominated by sea-level variations in response to atmospheric surface pressure loading, and therefore hides any dynamically relevant signal (Fig. 5.4). Interpretations are only possible by re-adding the atmospheric component as shown in the previous chapter. For the updated ESM under the modified IB-correction, however, a dynamic interpretation is instead possible. Note, that the dynamic responses of the ocean to quick changes in atmospheric surface pressure are of course also included in the updated ESM, since the modified IB-correction has been only applied a posteriori. Analyses for individual years indicate stationarity for both the original and the updated model (Fig. 5.6).

Similar conclusions can be drawn for the high-frequency part of the spectrum with periods between 1 and 30 days (Fig. 5.5). Whereas the oceanic component of the original ESM is hardly interpretable,

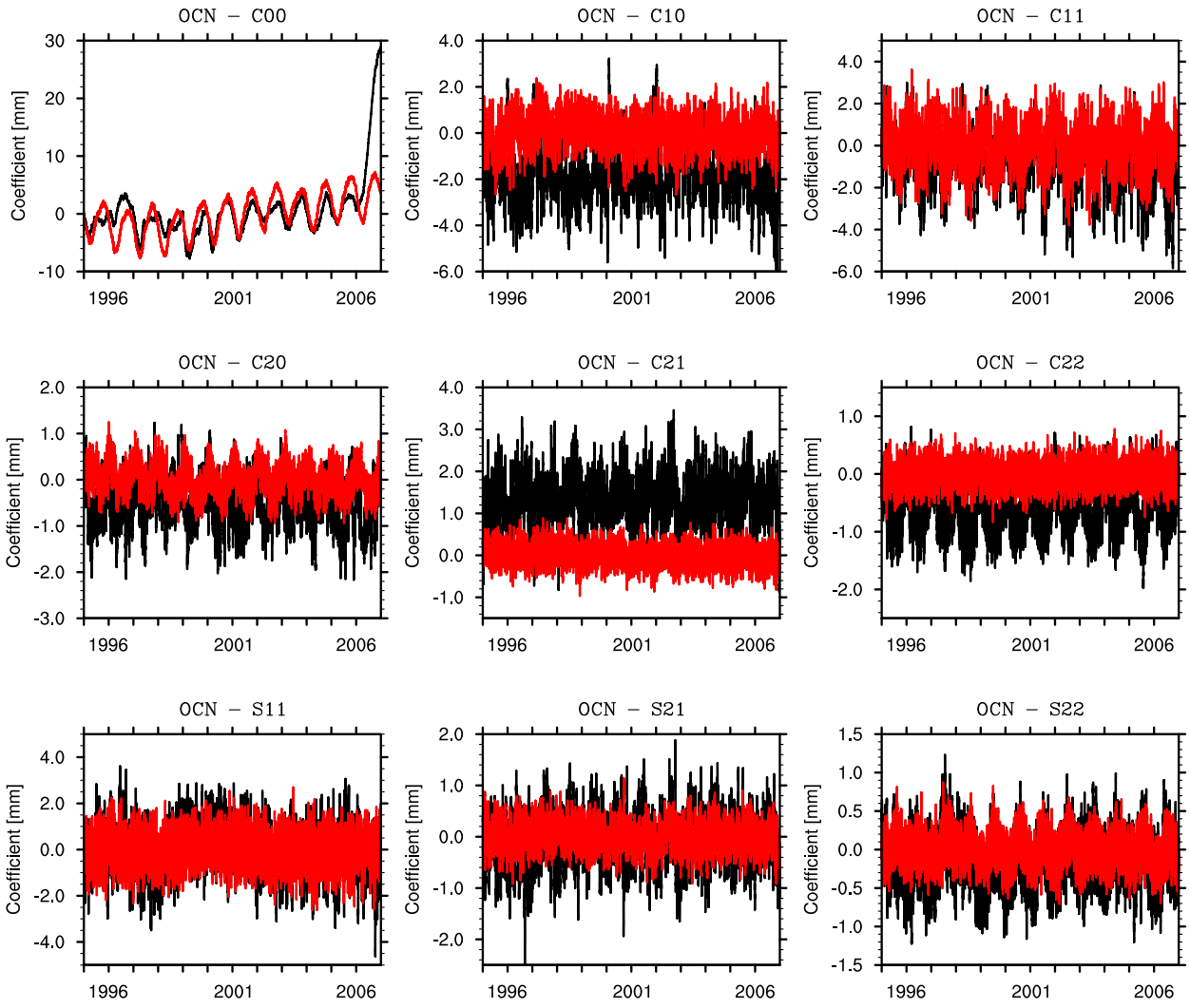

Figure 5.1: Time series (1995-2006) of low degree spherical harmonic coefficients of ocean-bottom pressure anomaly (O component). The coefficients from the original ESM are shown in black, that from the updated ESM in red.

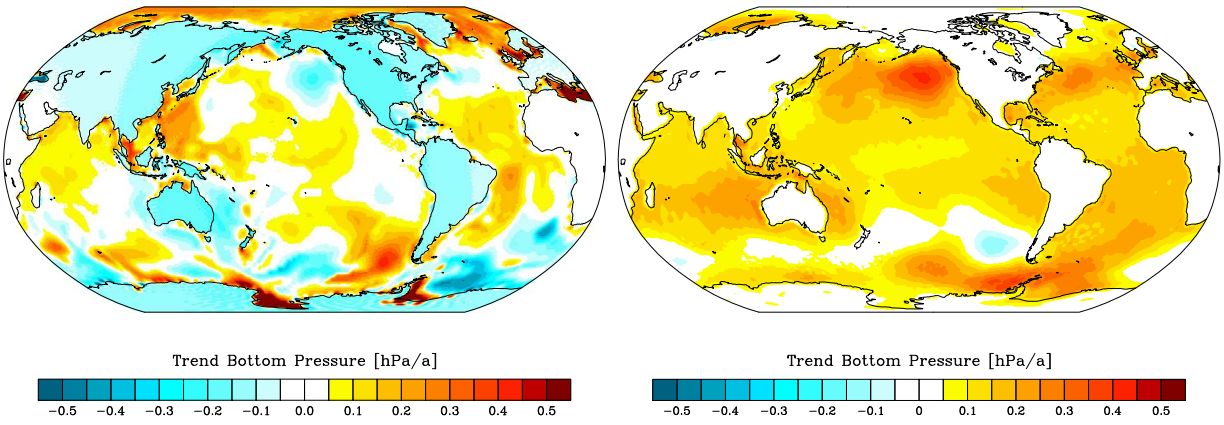

Figure 5.2: Local secular trends (1995-2006) at 0.5° spatial resolution obtained from the re-synthesized coefficients of the O component from the original (left) and updated ESM (right).

we identify typical ocean bottom pressure signals in the O component of the updated ESM under the modified IB-correction. The stationarity of the time-series is again confirmed by a analysis of the individual years (Fig. 5.7).

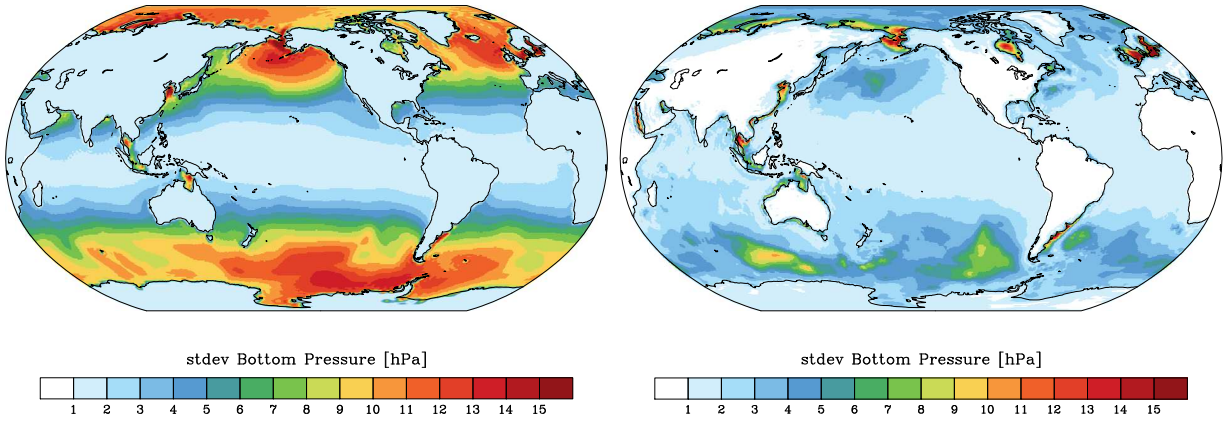

Figure 5.3: Standard deviation of ocean-bottom pressure anomaly (1995-2006) at 0.5° spatial resolution obtained from the re-synthesized and locally detrended coefficients of the O component from the original (left) and updated ESM (right).

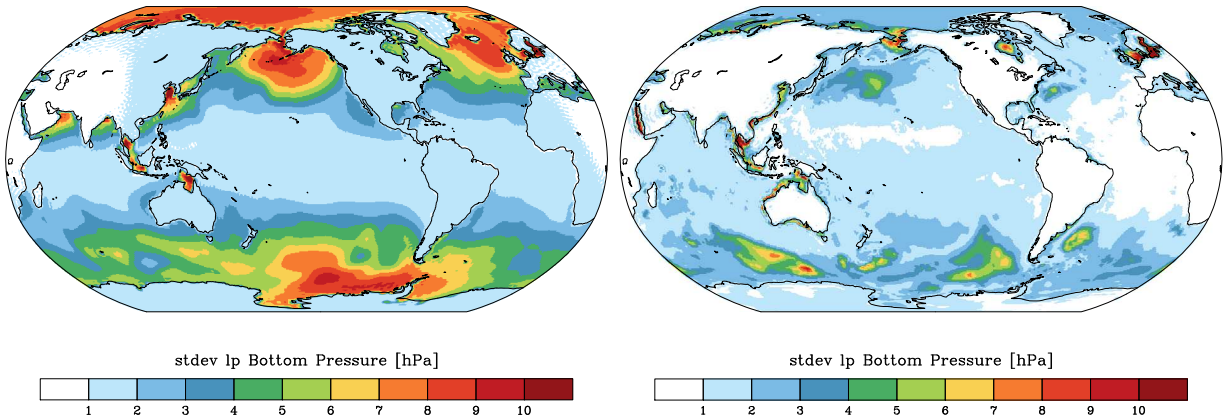

Figure 5.4: Standard deviation of ocean-bottom pressure anomaly (1995-2006) at 0.5° spatial resolution obtained from the re-synthesized, locally detrended and low-pass filtered (30 day cut-off) coefficients of the O component from the original (left) and updated ESM (right).

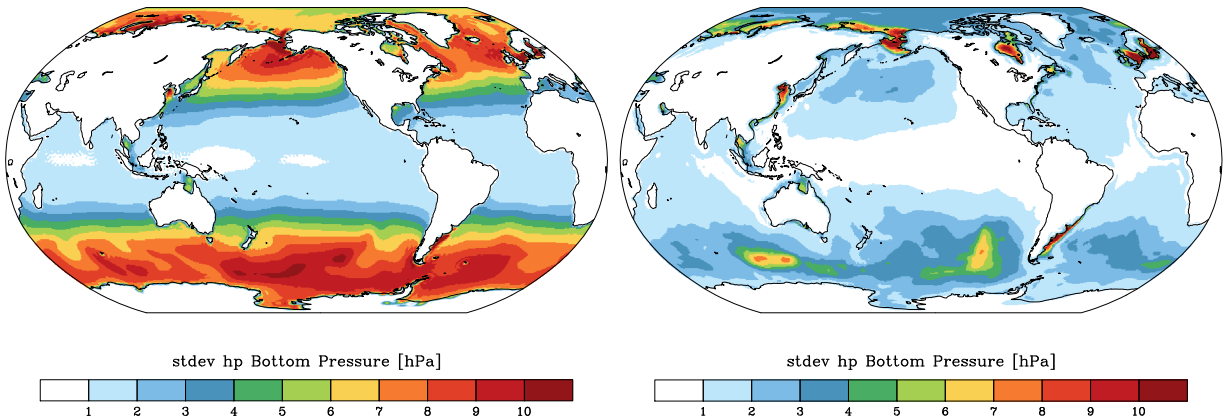

Figure 5.5: Standard deviation of ocean-bottom pressure anomaly (1995-2006) at 0.5° spatial resolution obtained from the re-synthesized, locally detrended and high-pass filtered (30 day cut-off) coefficients of the O component from the original (left) and updated ESM (right).

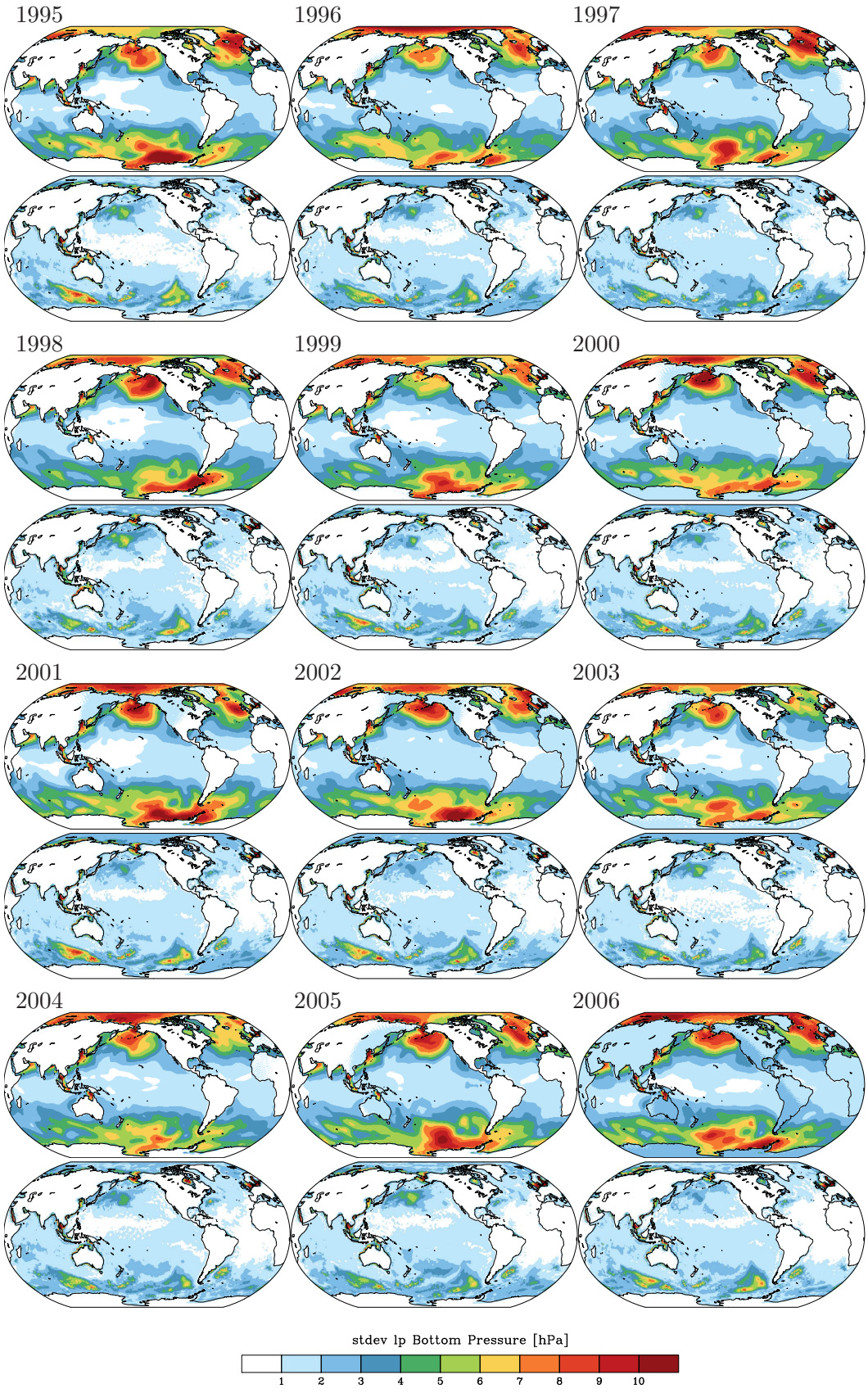

Figure 5.6: Standard deviation of ocean-bottom pressure anomaly at 0.5° spatial resolution obtained from the re-synthesized, locally detrended and low-pass filtered (30 day cut-off) coefficients of the O component from original (first) and updated ESM (second row) for each year between 1995 and 2006.

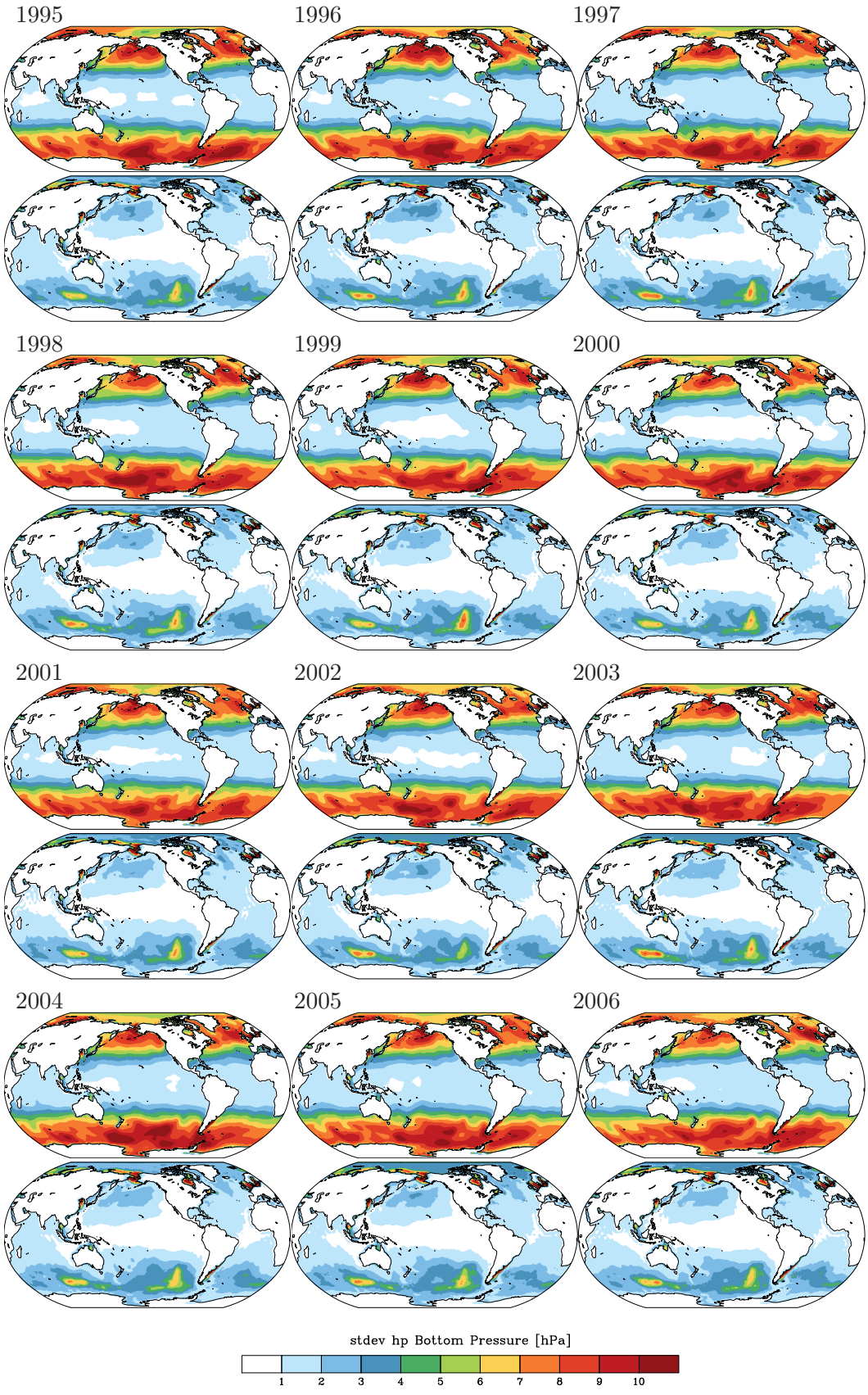

Figure 5.7: Standard deviation of ocean-bottom pressure anomaly at 0.5° spatial resolution obtained from the re-synthesized, locally detrended and high-pass filtered (30 day cut-off) coefficients of the O component from original (first) and updated ESM (second row) for each year between 1995 and 2006.

Chapter 6

Terrestrial Water Storage Changes

6.1 Global Low-Degree Coefficients

Time-series of low-degree coefficients of the H component of the original ESA ESM reveal a number of remarkable features (Fig. 6.1). This includes (i) a continuous and almost linear increase in total mass stored on the continents between 1995 and 2005, (ii) a sudden increase in total mass stored on the continents at the beginning of the year 2006, (iii) similar jumps at the beginning of 2006 also in other coefficients, (iv) a strong negative trend in C_{22}, and (v) dominant low-frequency variability in almost all coefficients considered. In contrast to this, the updated ESM does not show any of those features. Instead, most coefficients are characterised by a prominent seasonal cycle, and a very small trend.

6.2 Spatial Patterns of Trends and Variabilities

The spatial pattern of linear trends provide explanations to the trends seen in the low-degree spherical harmonics of the original ESA ESM discussed above (Fig. 6.2). For the original ESM, we find trends of up to 10 cm a^{-1} equivalent water thickness in many regions. Most trends are positive, but large parts of Africa instead show substantial drying of rates far too large to be plausible. Trends of the updated ESM are instead much smaller and show only trend magnitudes of about 1 cm a^{-1} that are coherent over larger regions, and might therefore indeed reflect low-frequency variability of the terrestrial branch of the global water cycle.

Variability plots of the original ESM are dominated by strong and isolated signals of more than 40 cm rms in Western Canada, Central Russia, and the Caucasus (Fig. 6.3), and we have no evidence from independent observations that such signals are indeed real. The updated ESM instead contains its largest variability over surface water bodies as the Lake Nasser in Egypt, or the Amazon river. Large-scale variability is otherwise concentrated in humid climates of the tropical latitudes. Low-pass filtered variability generally provides a similar picture (Fig. 6.4). From the yearly analyses, however, no particular year is substantially different from the others (Fig. 6.6), thereby suggesting that it is in particular low-frequency variability beyond the linear trend that causes the strong variability pattern in Fig. 6.4.

For the high-frequency part of TWS, we once more identify substantially stronger signals in the original ESM when compared to the update. This variability, however, primarily originates from three years only (Fig. 6.7). We note strong signals for 1995 that subsequently decline over the following years until 2004, where high-frequency variability is fairly comparable with the updated ESM. In 2005, however, high-frequency variability jumps up again to a level even higher than in

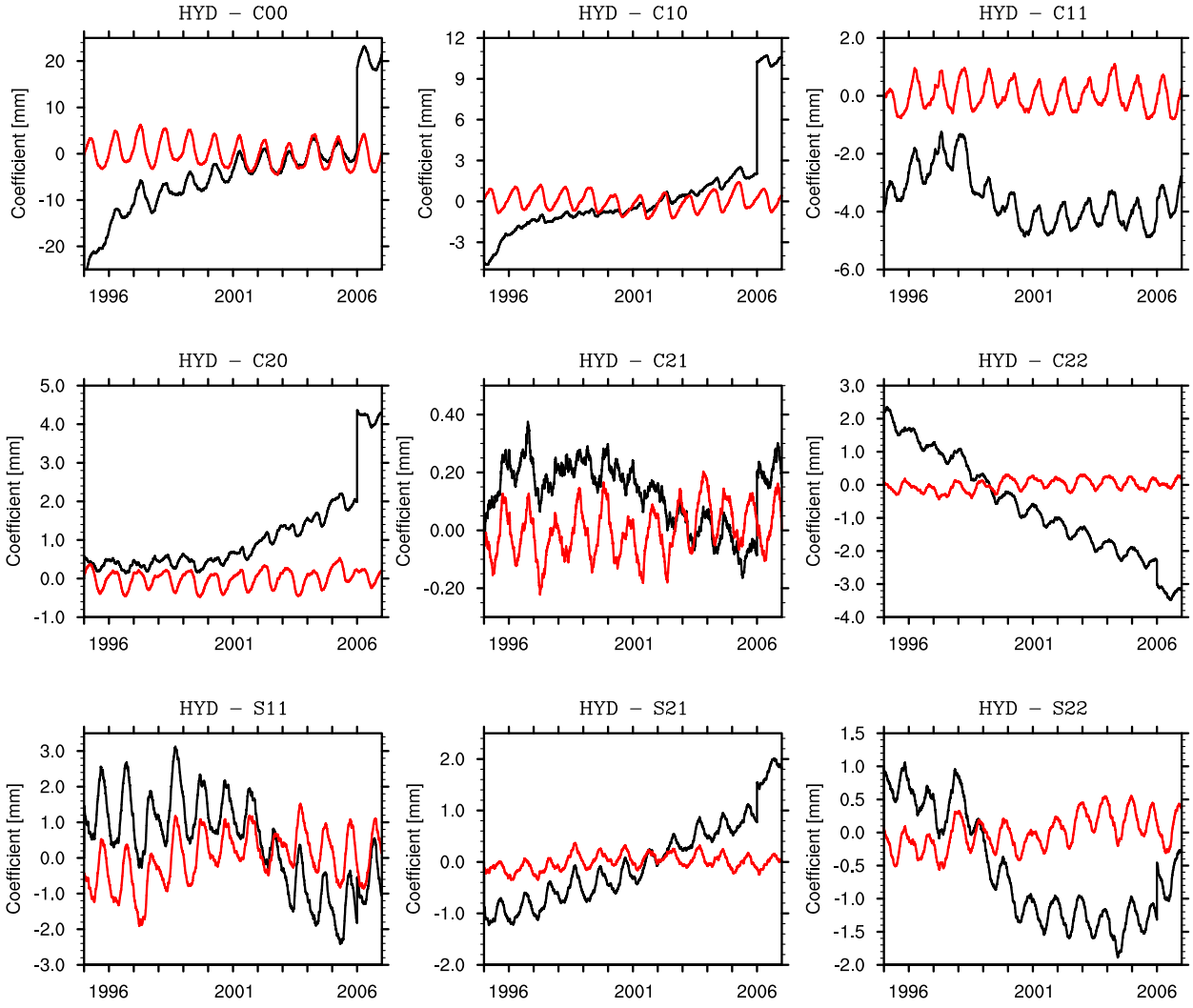

Figure 6.1: Time series (1995-2006) of low degree spherical harmonic coefficients of terrestrial water storage anomaly (H component). The coefficients from the original ESM are shown in black, that from the updated ESM in red.

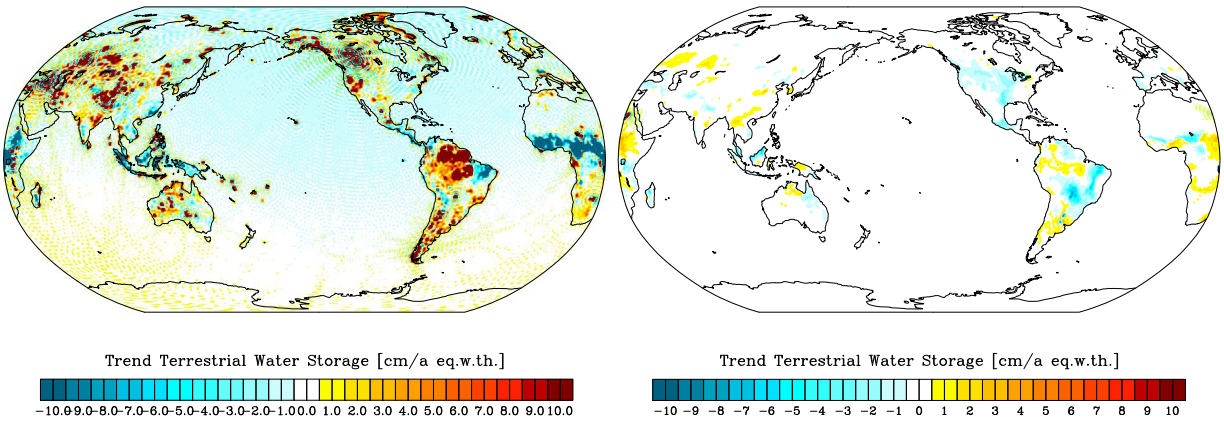

Figure 6.2: Local secular trends (1995-2006) at 0.5° spatial resolution obtained from the re-synthesized coefficients of the H component from the original (left) and updated ESM (right).

1995, and remains high during the final year 2006. Based on this evidence for missing stationarity of those time-series, the application of this component of the original ESA ESM for satellite simulation studies cannot be recommended.

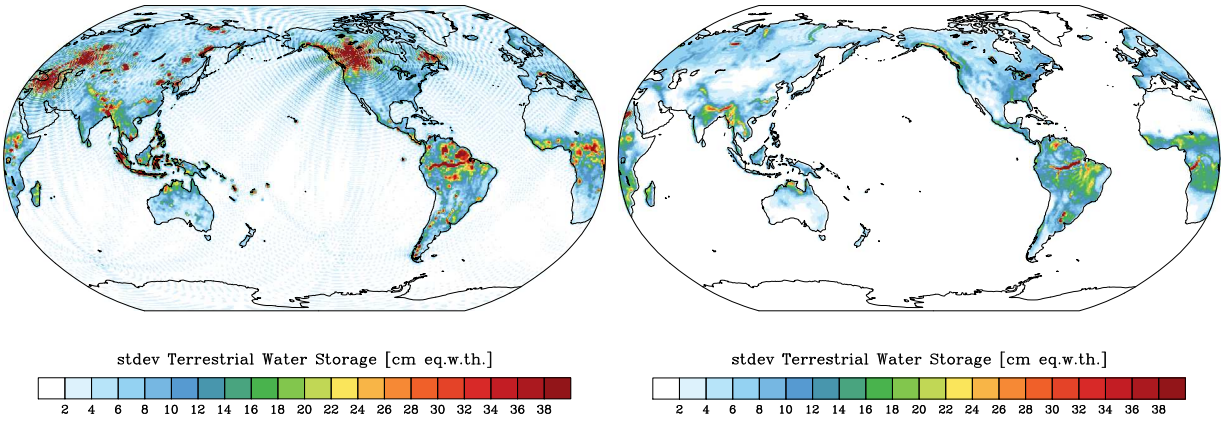

Figure 6.3: Standard deviation of terrestrial water storage anomaly (1995-2006) at 0.5° spatial resolution obtained from the re-synthesized and locally detrended coefficients of the H component from the original (left) and updated ESM (right).

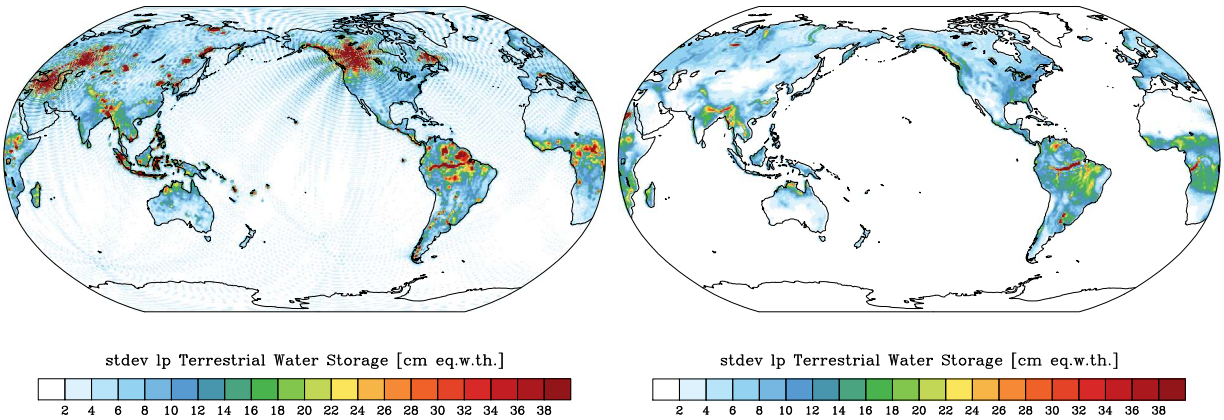

Figure 6.4: Standard deviation of terrestrial water storage anomaly (1995-2006) at 0.5° spatial resolution obtained from the re-synthesized, locally detrended and low-pass filtered (30 day cut-off) coefficients of the H component from the original (left) and updated ESM (right).

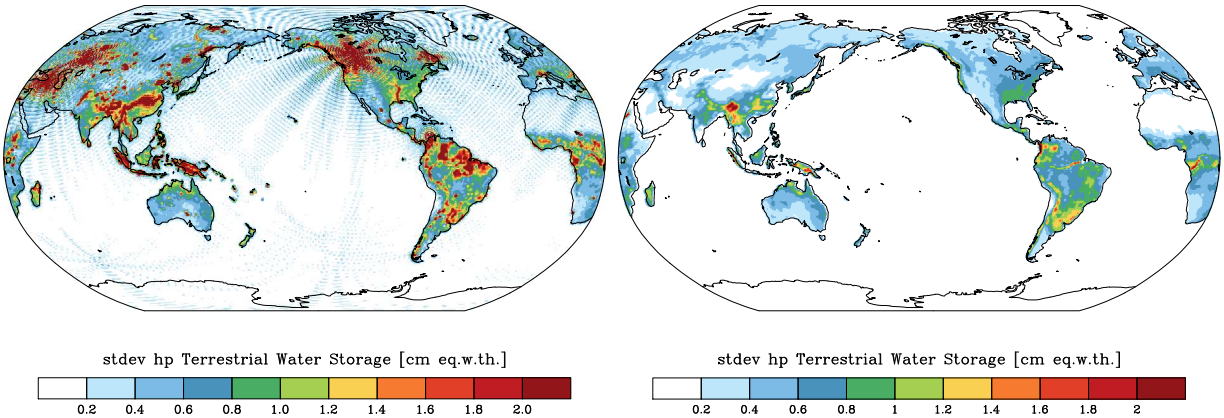

Figure 6.5: Standard deviation of terrestrial water storage anomaly (1995-2006) at 0.5° spatial resolution obtained from the re-synthesized, locally detrended and high-pass filtered (30 day cut-off) coefficients of the H component from the original (left) and updated ESM (right).

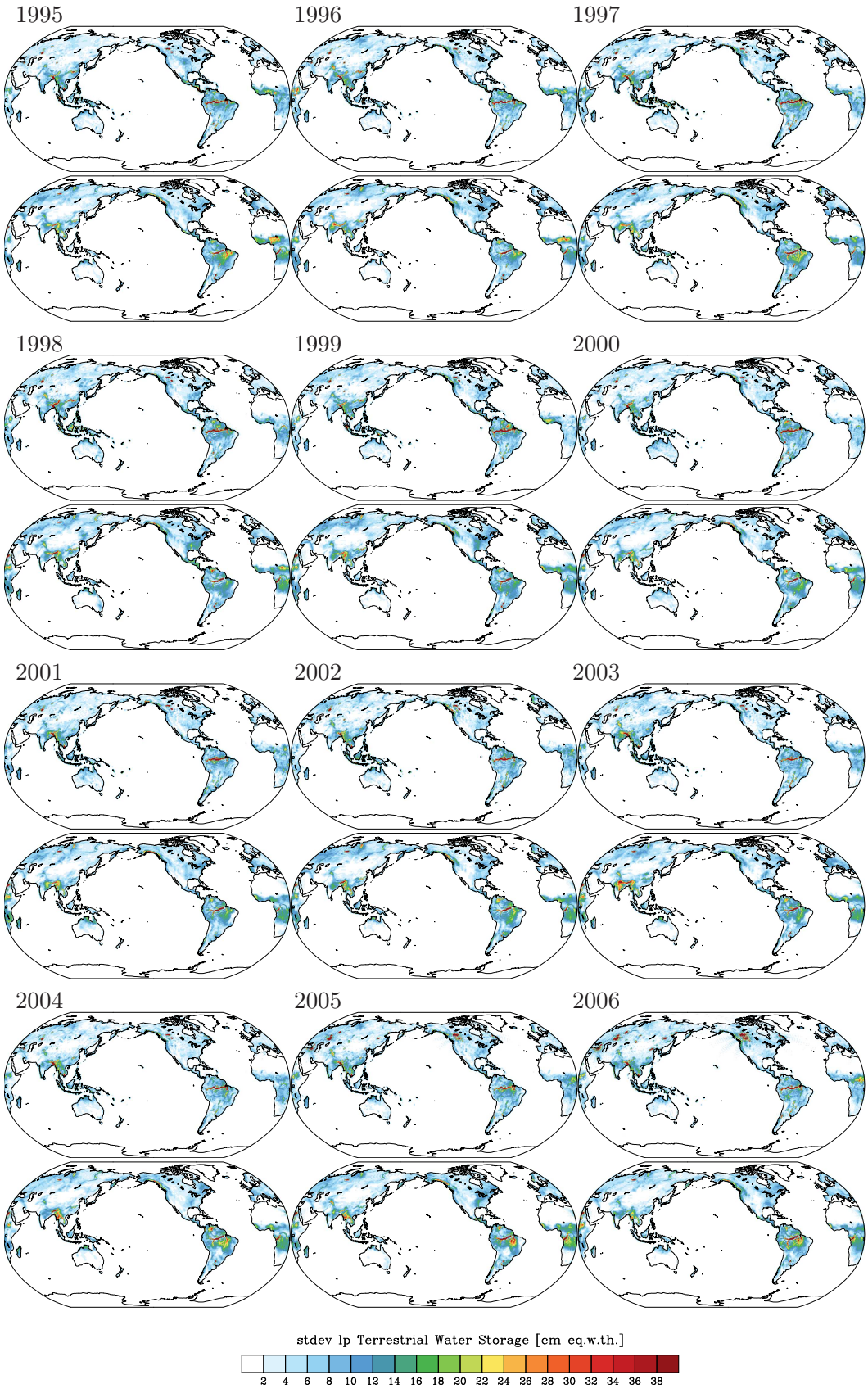

Figure 6.6: Standard deviation of terrestrial water storage anomaly at 0.5° spatial resolution obtained from the re-synthesized, locally detrended and low-pass filtered (30 day cut-off) coefficients of the H component from original (first) and updated ESM (second row) for each year between 1995 and 2006.

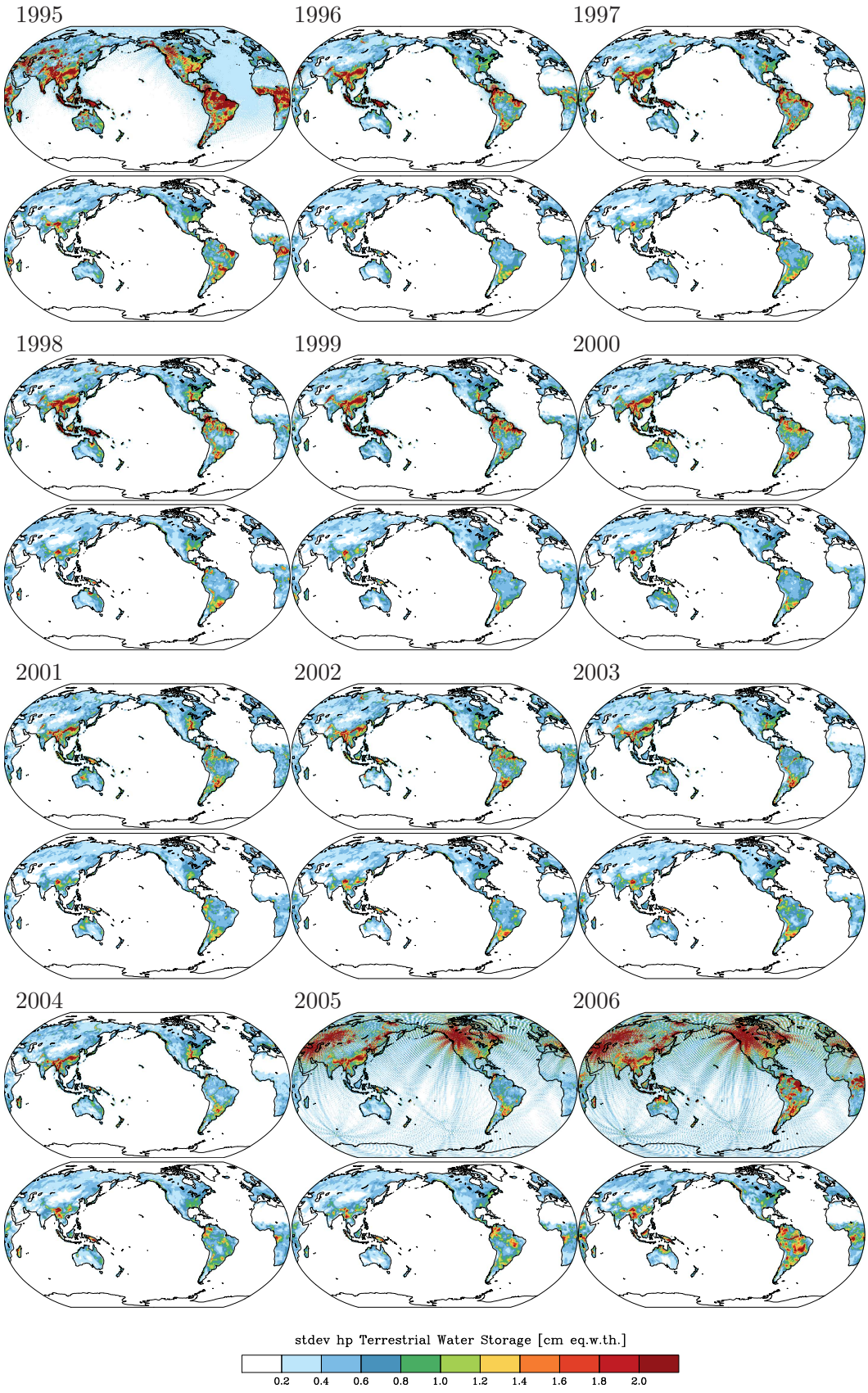

Figure 6.7: Standard deviation of terrestrial water storage anomaly at 0.5° spatial resolution obtained from the re-synthesized, locally detrended and high-pass filtered (30 day cut-off) coefficients of the H component from original (first) and updated ESM (second row) for each year between 1995 and 2006.

Chapter 7

Continental Ice-Sheets

7.1 Global Low-Degree Coefficients

Time-series of low-degree spherical harmonics reveal a number of differences between the original and the updated ESM (Fig. 7.1). The seasonal cycle present in many of the coefficients is reduced in the update. Trends, however, are partly increased, as, for example in C_{00} and C_{22}. We argue that this might be due to the inclusion of mountain glacier mass trends in the component I of the updated ESM. In the original version, mountain glaciers were included into the H component.

7.2 Spatial Patterns of Trends and Variabilities

Spatial patterns of linear trends of both models are identical over Greenland and Antarctica, since those signal parts have been taken from the original model also for the update (Fig. 7.2). In addition, the positions of the mountain glacier mass trends included into the update are visible.

Variabilities (Fig. 7.3) exhibit stronger leakage into the oceans in particular around Greenland, but otherwise show similar signal magnitudes that are concentrated primarily in coastal regions of both Southern Greenland and the West-Antarctic. Low-pass filtered variability plots (Fig. 7.4) exhibit similar features, and yearly analyses (Fig. 7.6) do not provide evidence for any anomalous variations in any particular year.

High-frequency variability at periods between 1 and 30 days is generally small for the cryosphere and fairly consistent in both model versions (Fig. 7.5). From the yearly analyses, we note slightly increased variability in the first and in the last year of the time-series, which might be related to model initialization or filtering effects. However, those signals are evaluated as sufficiently small so that stationarity of the time-series still is ensured.

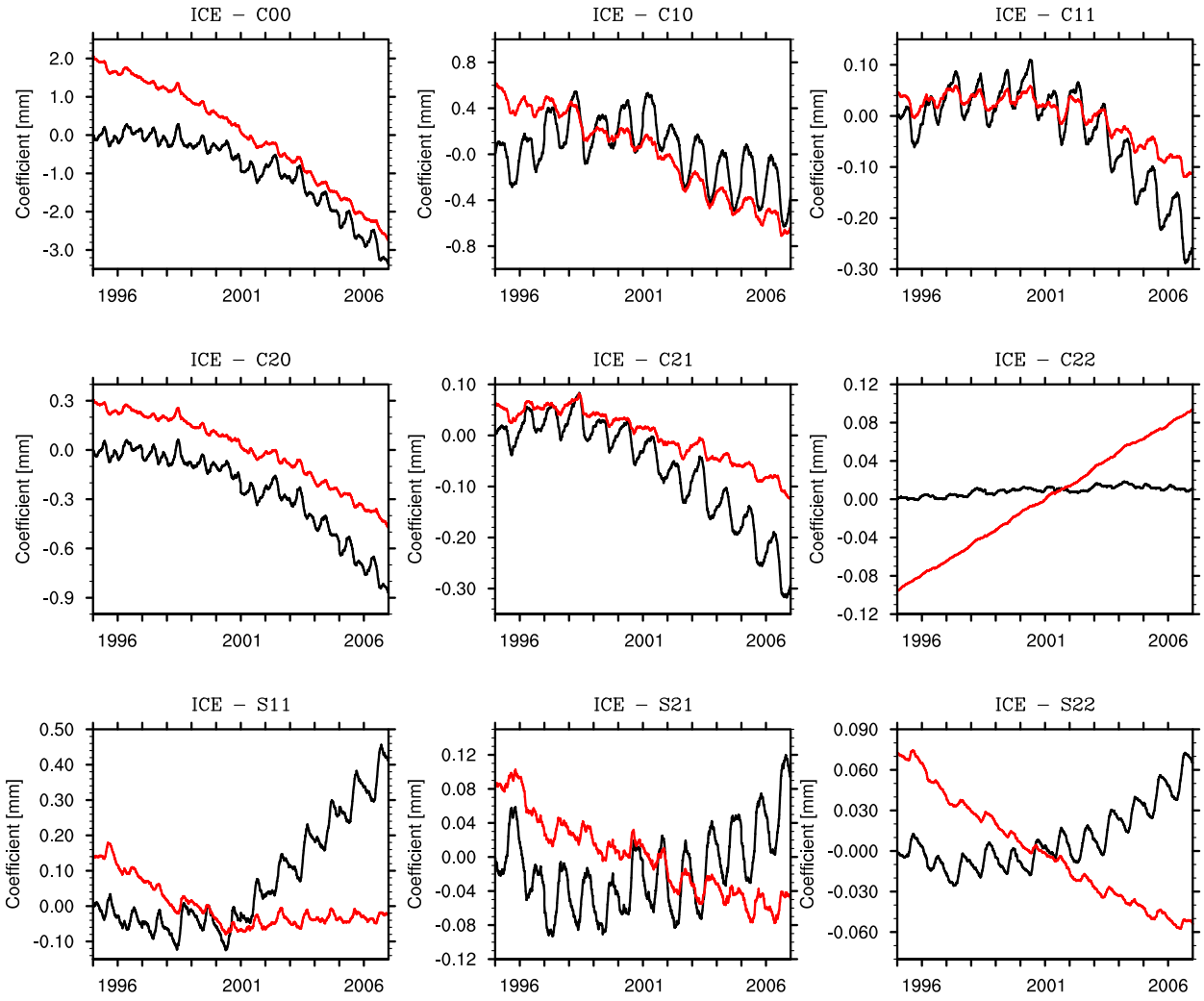

Figure 7.1: Time series (1995-2006) of low degree spherical harmonic coefficients of ice-mass anomaly (I component). The coefficients from the original ESM are shown in black, that from the updated ESM in red.

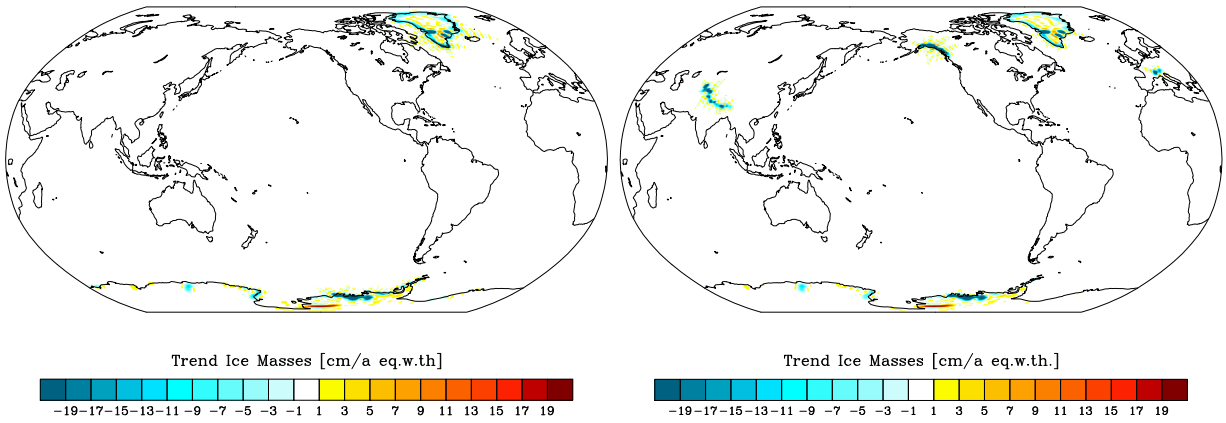

Figure 7.2: Local secular trends (1995-2006) at 0.5° spatial resolution obtained from the re-synthesized coefficients of the I component from the original (left) and updated ESM (right).

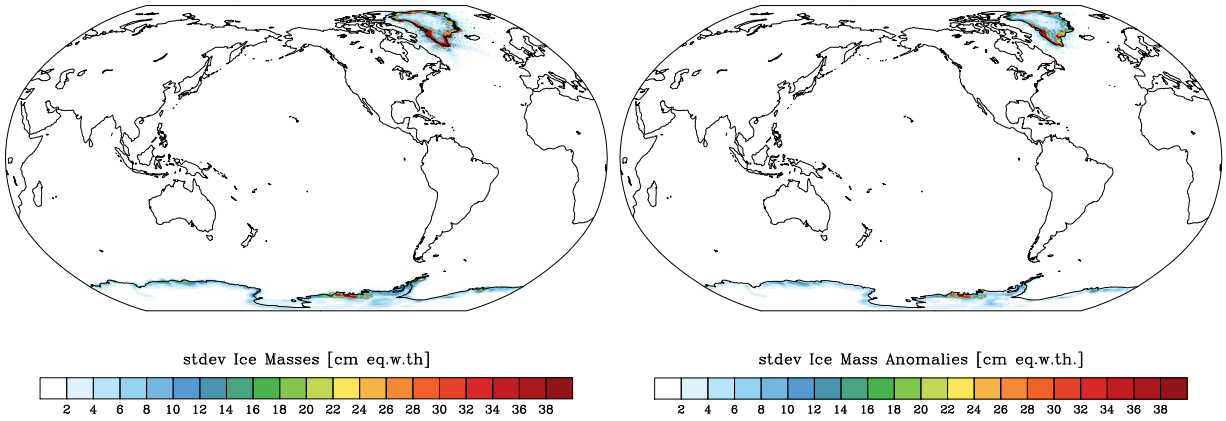

Figure 7.3: Standard deviation of ice-mass anomaly (1995-2006) at 0.5° spatial resolution obtained from the re-synthesized and locally detrended coefficients of the I component from the original (left) and updated ESM (right).

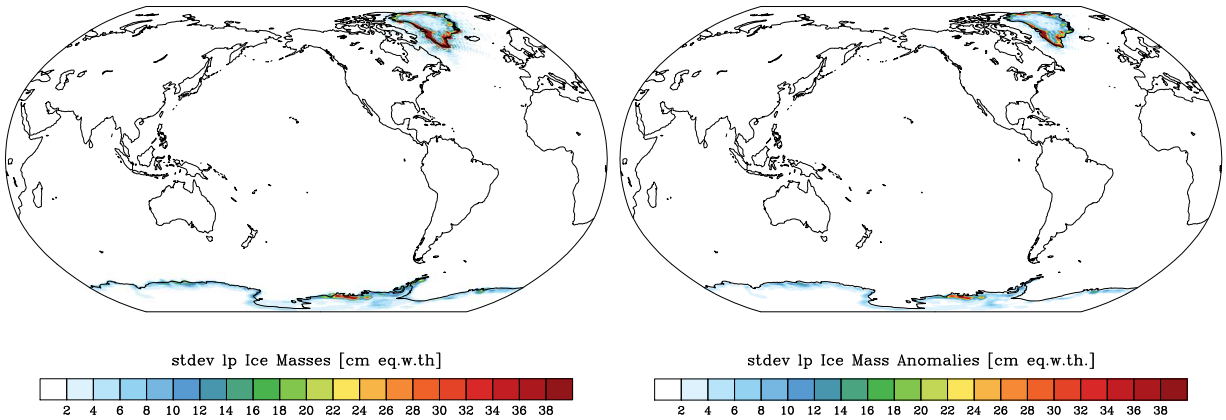

Figure 7.4: Standard deviation of ice-mass anomaly (1995-2006) at 0.5° spatial resolution obtained from the re-synthesized, locally detrended and low-pass filtered (30 day cut-off) coefficients of the I component from the original (left) and updated ESM (right).

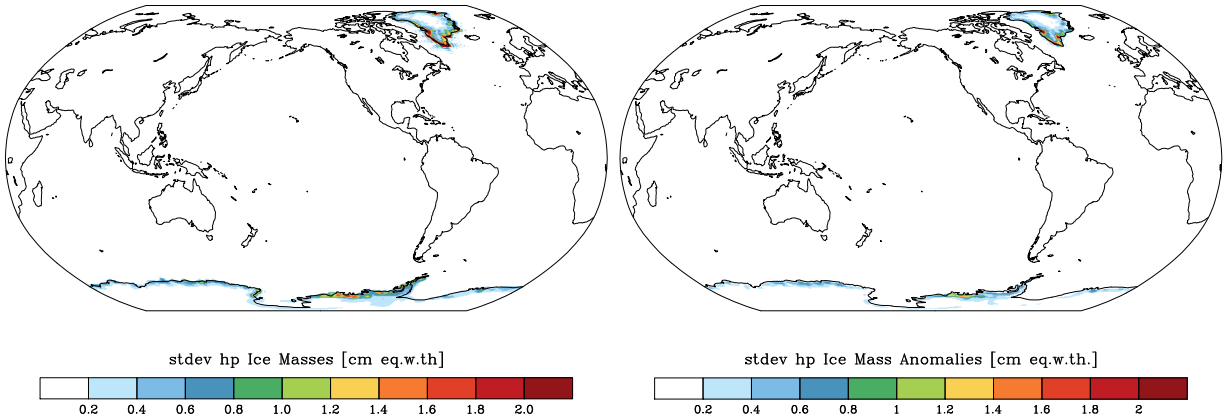

Figure 7.5: Standard deviation of ice-mass anomaly (1995-2006) at 0.5° spatial resolution obtained from the re-synthesized, locally detrended and high-pass filtered (30 day cut-off) coefficients of the I component from the original (left) and updated ESM (right).

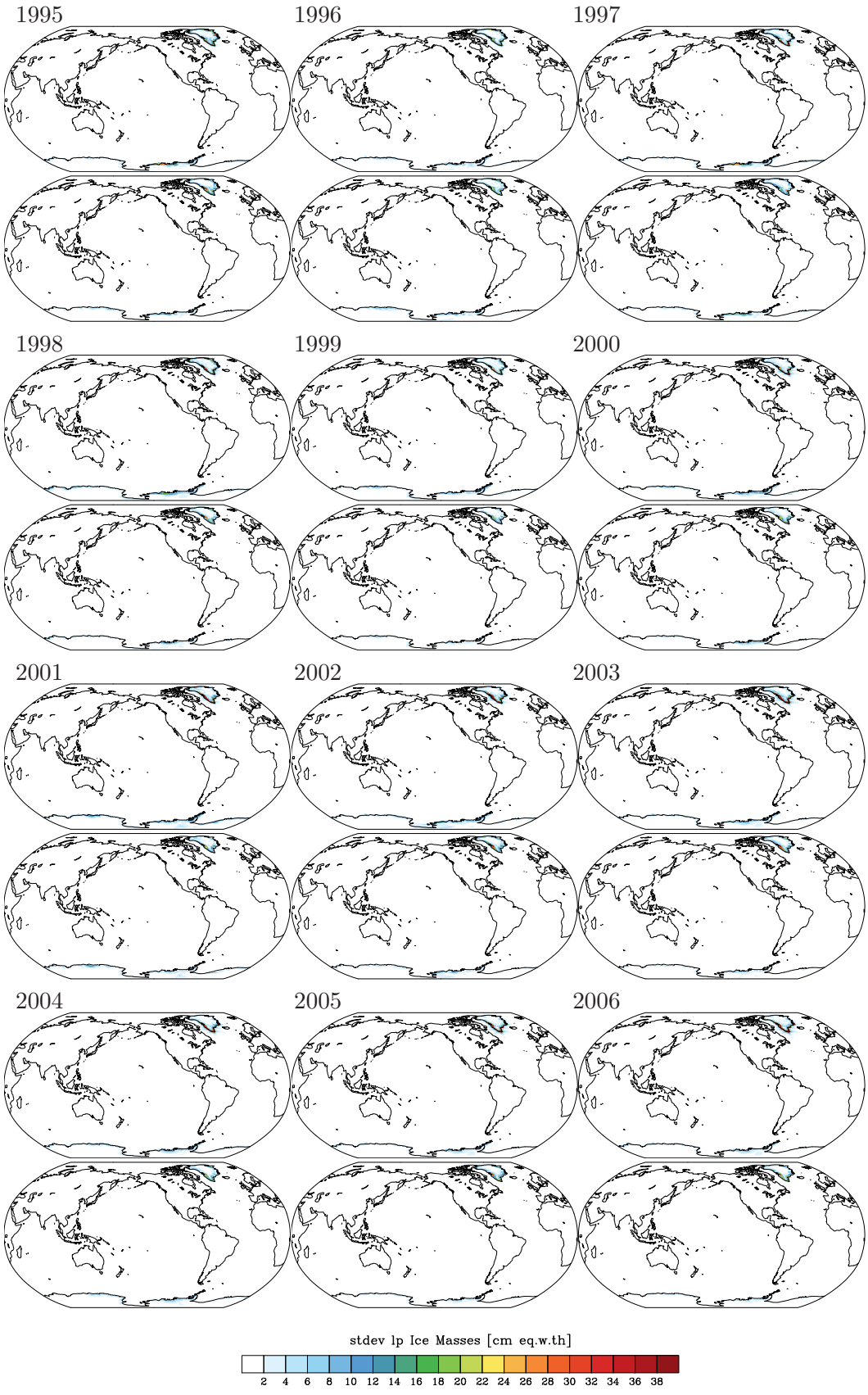

Figure 7.6: Standard deviation of ice-mass anomaly at 0.5° spatial resolution obtained from the re-synthesized, locally detrended and low-pass filtered (30 day cut-off) coefficients of the I component from original (first) and updated ESM (second row) for each year between 1995 and 2006.

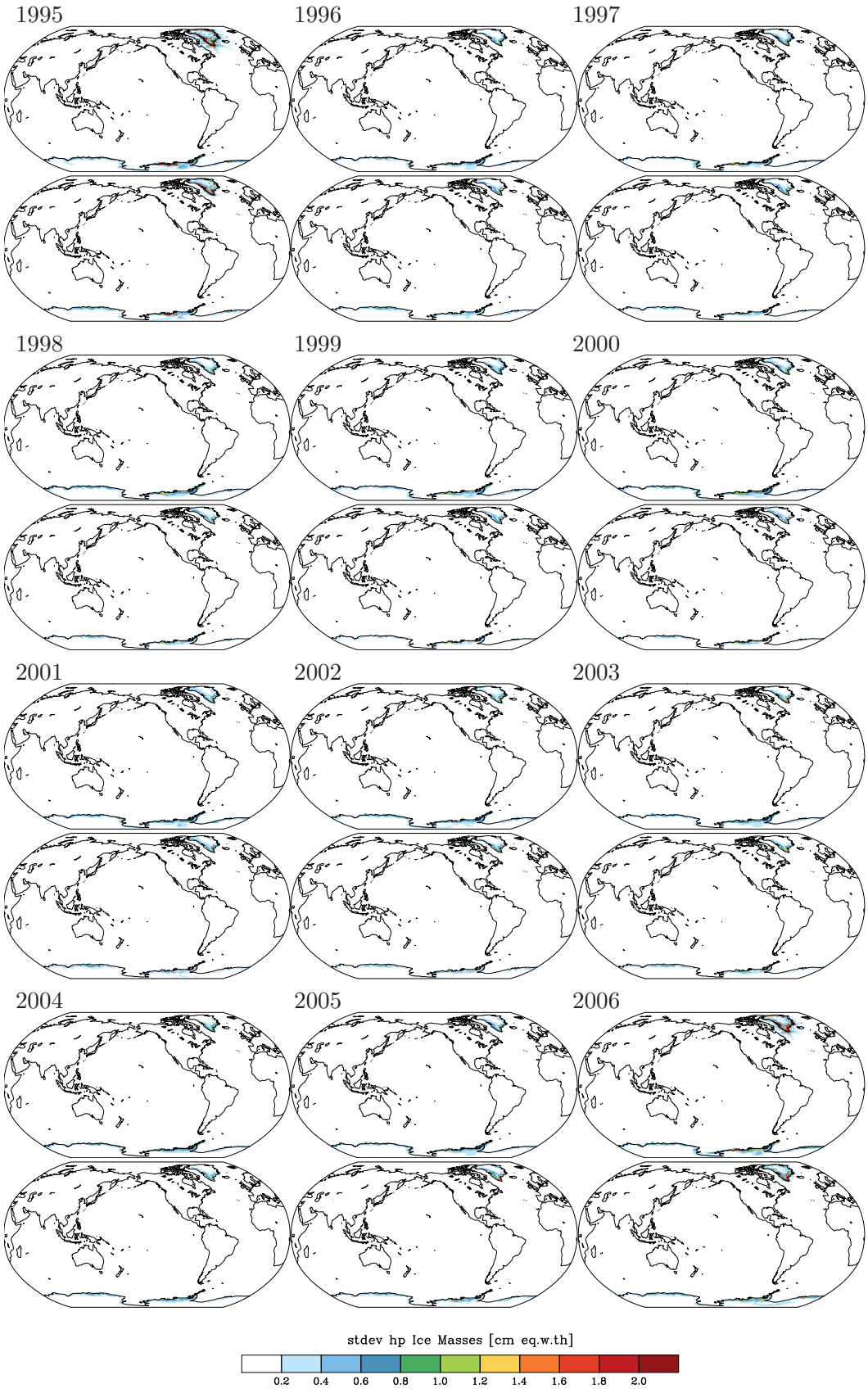

Figure 7.7: Standard deviation of ice-mass anomaly at 0.5° spatial resolution obtained from the re-synthesized, locally detrended and high-pass filtered (30 day cut-off) coefficients of the I component from original (first) and updated ESM (second row) for each year between 1995 and 2006.

Chapter 8

Glacial Isostatic Adjustment and Co- and Post-Seismic Deformations

8.1 Global Low-Degree Coefficients

The total mass anomaly in the solid Earth is not constant in the original ESM, but drifts in time and shows an effect due to the Sumatra-Andaman Earth quake (Fig. 8.1). This is not realistic, since deformations cause only a re-distribution of mass. In the updated ESM, C_{00} remains constant. Degree-1 terms instead only reveal a drift in the updated model version, since they have been specifically included following Klemann & Martinec (2011).

8.2 Spatial Patterns of Trends and Variabilities

For the trend pattern, we find largely similar pattern for both the original and the updated ESM (Fig. 8.2) with dominating positive trends over the regions of the previous ice domes. Variability is dominated by the co-seismic deformation of the Sumatra-Andaman Earth quake (8.3), where only spatial leakage caused by a rather poor patching of the Earth quake model into the GIA model has been reduced in the updated model version (Fig. 8.4).

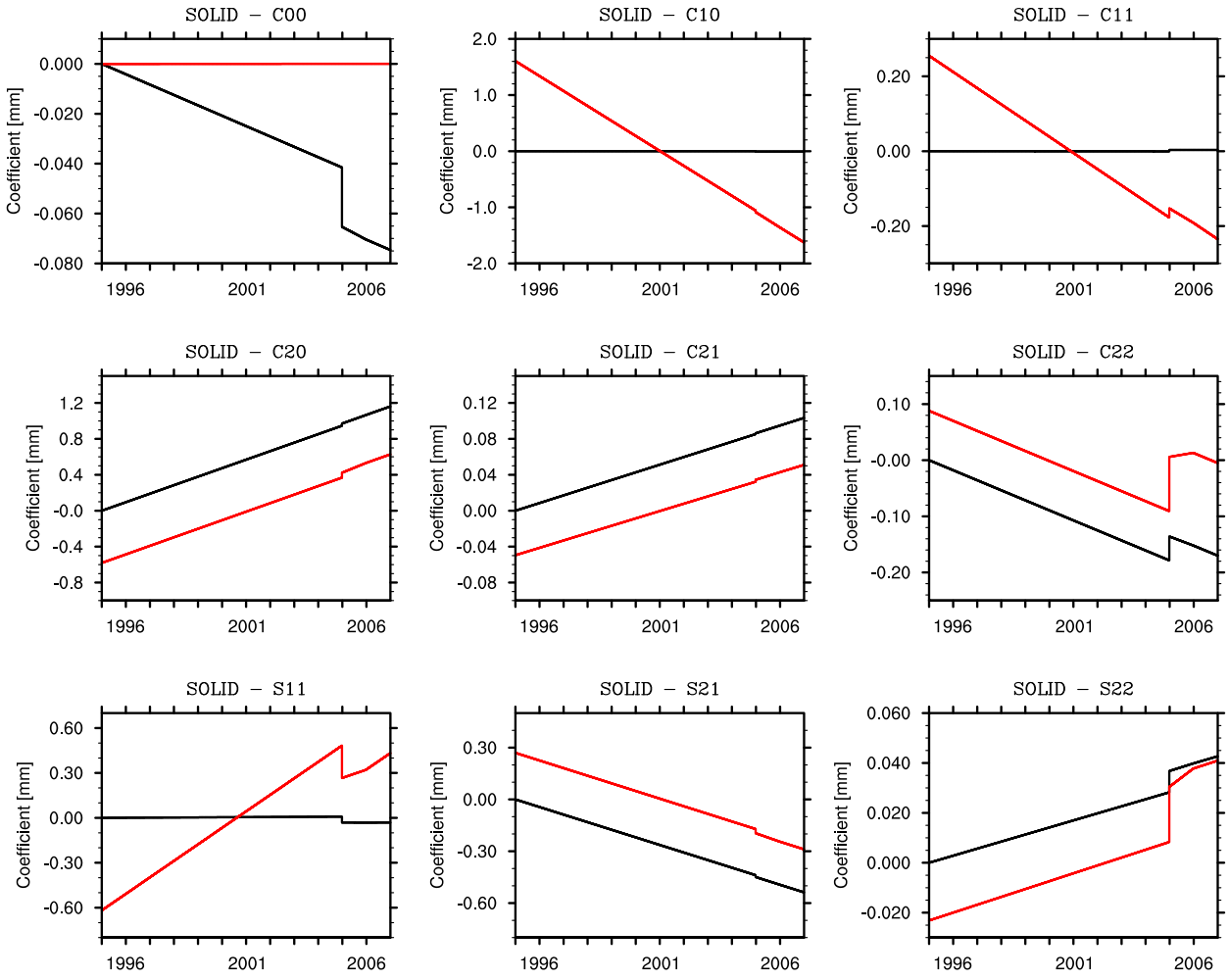

Figure 8.1: Time series (1995-2006) of low degree spherical harmonic coefficients of solid-earth effects (S component). The coefficients from the original ESM are shown in black, that from the updated ESM in red.

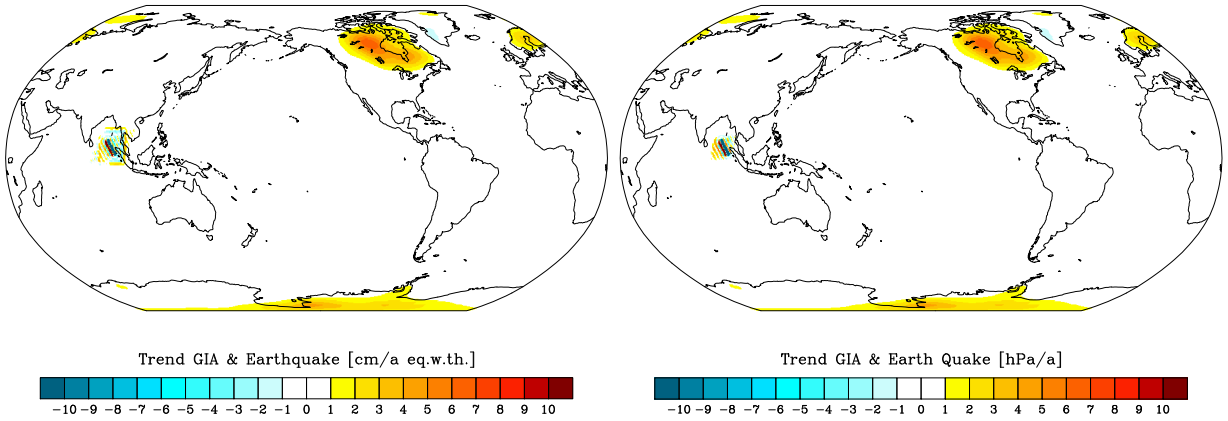

Figure 8.2: Local secular trends (1995-2006) at 0.5° spatial resolution obtained from the re-synthesized coefficients of the S component from the original (left) and updated ESM (right).

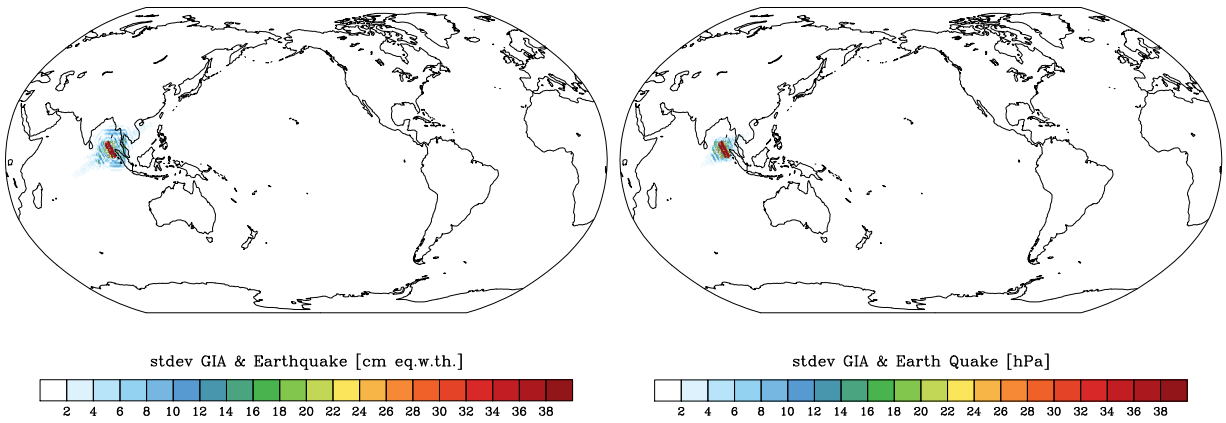

Figure 8.3: Standard deviation of solid-earth effects (1995-2006) at 0.5° spatial resolution obtained from the re-synthesized and locally detrended coefficients of the S component from the original (left) and updated ESM (right).

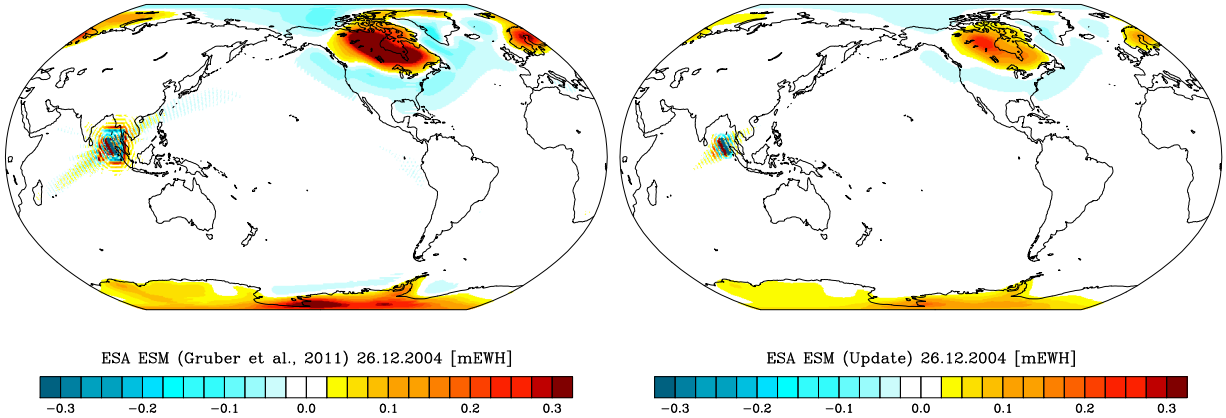

Figure 8.4: Coseismic signal at 0.5° spatial resolution obtained from the re-synthesized and S component from the original (left) and updated ESM (right).

Chapter 9

Characteristics of AOHIS

9.1 Global Low-Degree Coefficients

Based on time-series of the low-degree coefficients of the combined component AOHIS (Fig. 9.1), we note that the global mass in the system is nearly conserved in the updated ESM. Moreover, other coefficients of the updated ESM reveal no or very small trends, and do not contain any low-frequency variability, as it is found instead in the original ESM in some coefficients.

9.2 Spatial Patterns of Trends and Variabilities

Spatial pattern of linear trends of the updated ESM are dominated by GIA and ice mass signals and slightly smaller long-term trends in terrestrially stored water that are typically coherent over large spatial scales (Fig. 9.2). In contrast to this, the original ESM is characterised by strong but patchy trends in TWS that partly even dominate GIA, a feature that is not supported by any satellite or in-situ gravity observation available today.

The strongest low-frequency variability in the updated model version originates from surface water bodies like large lakes or reservoirs, or the major river channels (Fig. 9.3). In addition, substantial variabilitity in surface mass balance and ice dynamics at the margins of the continental ice-sheets is visible. The variability of the original model instead is dominated by isolated peaks in mountaineous regions in Canada, Russia, and the Caucasus, that are not supported by observations and therefore believed to be largely artificial. The low-pass filtered variabilities at periods longer than 30 days generally reveal similar pictures (Fig. 9.4).

High-frequency variations in the updated model version are dominated by atmospheric pressure over the continents, and ocean-bottom pressure variability in response to the time-varying winds and surface pressure in oceanic regions (Fig. 9.5). Results from both model versions are generally consistent, but we note slightly steeper spatial gradients in the updated ESM when compared to the original model by Gruber *et al.* (2011).

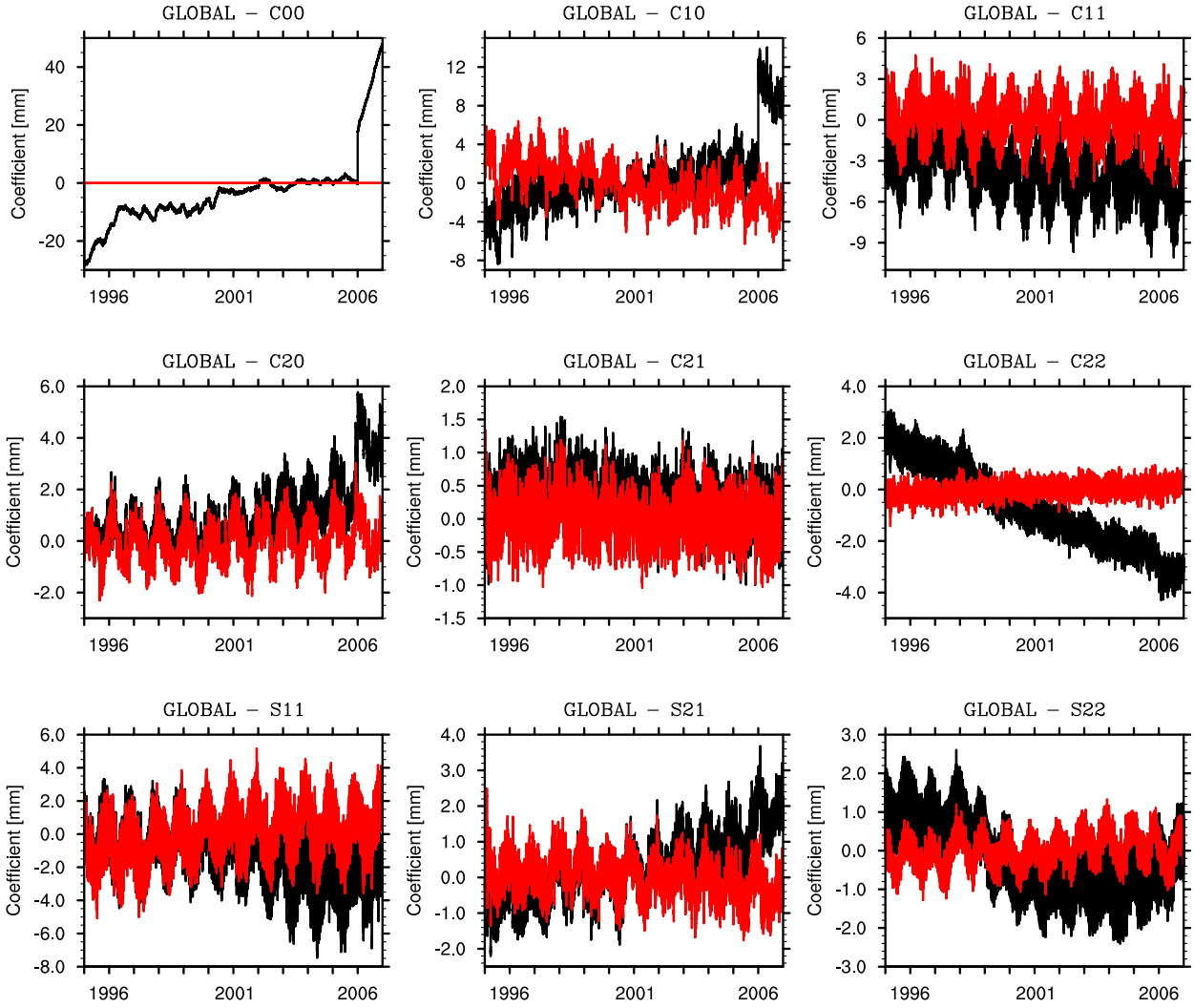

Figure 9.1: Time series (1995-2006) of low degree spherical harmonic coefficients of total pressure anomaly (AOHIS component). The coefficients from the original ESM are shown in black, that from the updated ESM in red.

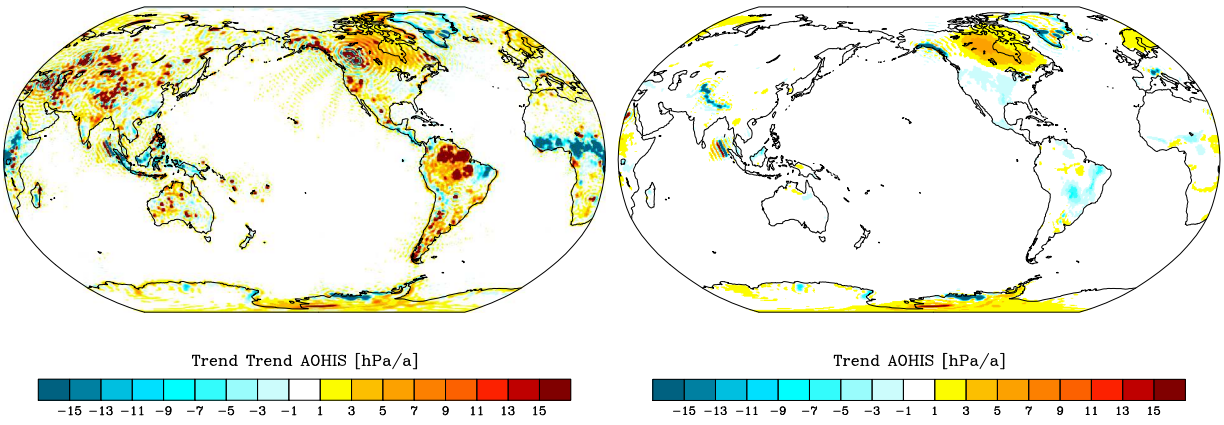

Figure 9.2: Local secular trends (1995-2006) at 0.5° spatial resolution obtained from the re-synthesized coefficients of the AOHIS component from the original (left) and updated ESM (right).

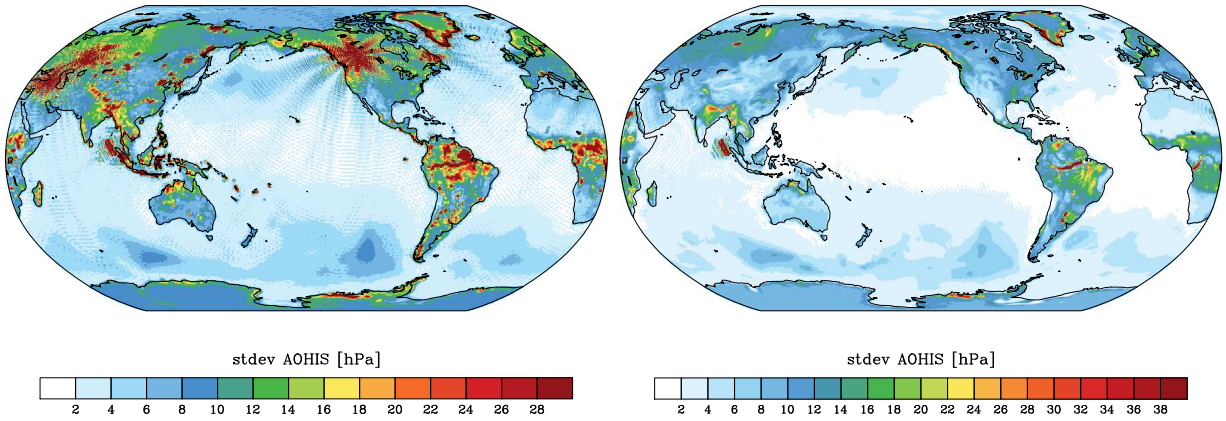

Figure 9.3: Standard deviation of total pressure anomaly (1995-2006) at 0.5° spatial resolution obtained from the re-synthesized and locally detrended coefficients of the AOHIS component from the original (left) and updated ESM (right).

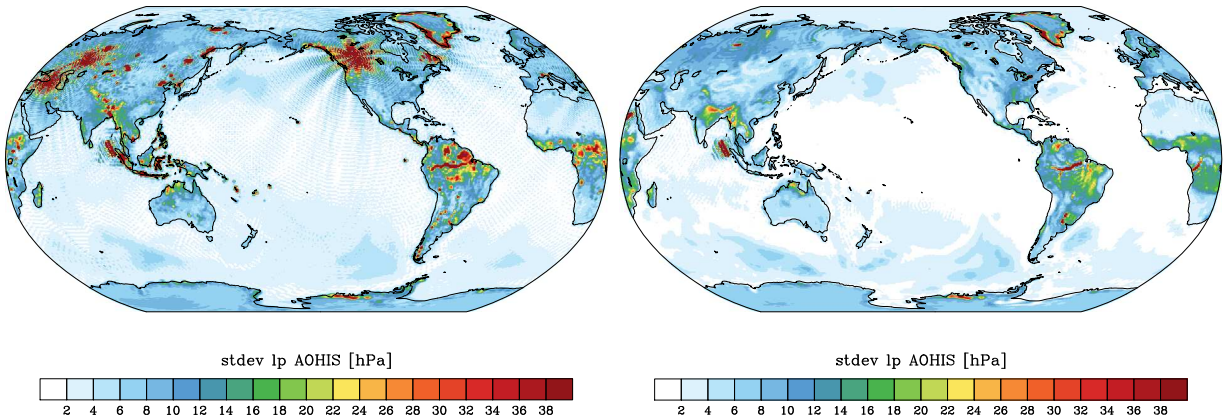

Figure 9.4: Standard deviation of total pressure anomaly (1995-2006) at 0.5° spatial resolution obtained from the re-synthesized, locally detrended and low-pass filtered (30 day cut-off) coefficients of the AOHIS component from the original (left) and updated ESM (right).

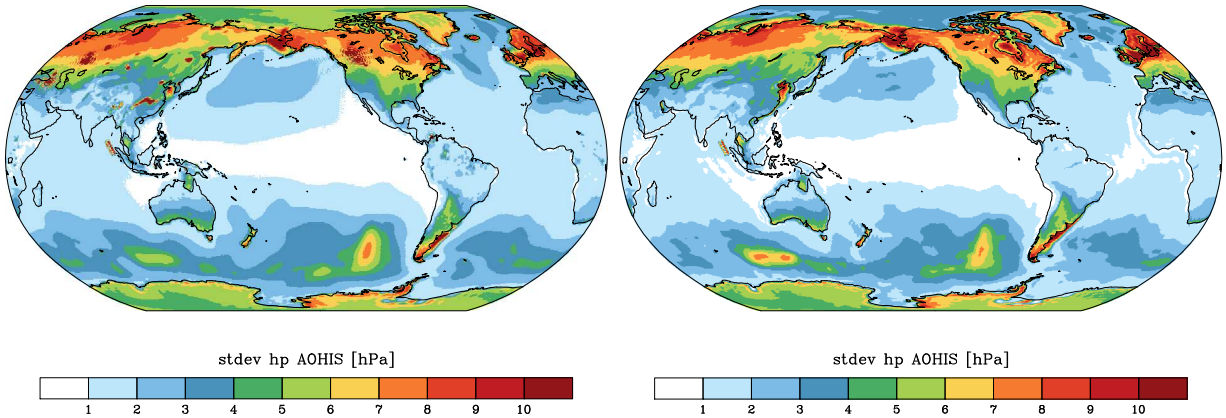

Figure 9.5: Standard deviation of total pressure anomaly (1995-2006) at 0.5° spatial resolution obtained from the re-synthesized, locally detrended and high-pass filtered (30 day cut-off) coefficients of the AOHIS component from the original (left) and updated ESM (right).

Chapter 10

Tides and Sub-Diurnal Atmospheric and Oceanic Variability

10.1 Atmospheric Tides

Spatial pattern of the atmospheric tides S1(p) over the continents are largely consistent between the original and the updated ESM (Fig. 10.1). Signal amplitudes approach 1 hPa and reveal small-scale characteristics in particular in tropical latitudes, where local convective activity contributes to variations at exactly diurnal periods. Over the oceans, instead, we note differences between the original model and the update. Here, resonances in the ocean model are critically dependent on bathymetry and thus spatial resolution, thereby causing modifications in the amphidromic systems. Nevertheless, both model version can be regarded as realistic within the requirement limits of a satellite gravity mission simulation study.

For the atmospheric tide S2(p) we note that this signal aliases into a standing wave due to the Nyquist criterion (Fig. 10.2). A semi-diurnal signal sampled at an interval of 6 hours is therefore not a realistic representation. Semi-diurnal variability has been therefore removed from the updated ESM.

10.2 Sub-Diurnal Variability

Sub-daily variability as obtained by subtracting daily running mean values from the time-series of A+O prior to the calculation of rms values is fairly comparable between both versions of ESA ESM (Fig. 10.3). Moreover, analysis of individual years do not reveal differences between individual years that go beyond natural climate and weather variability, leading to the conclusion that the sub-daily signals are equally well represented in both versions of ESA ESM.

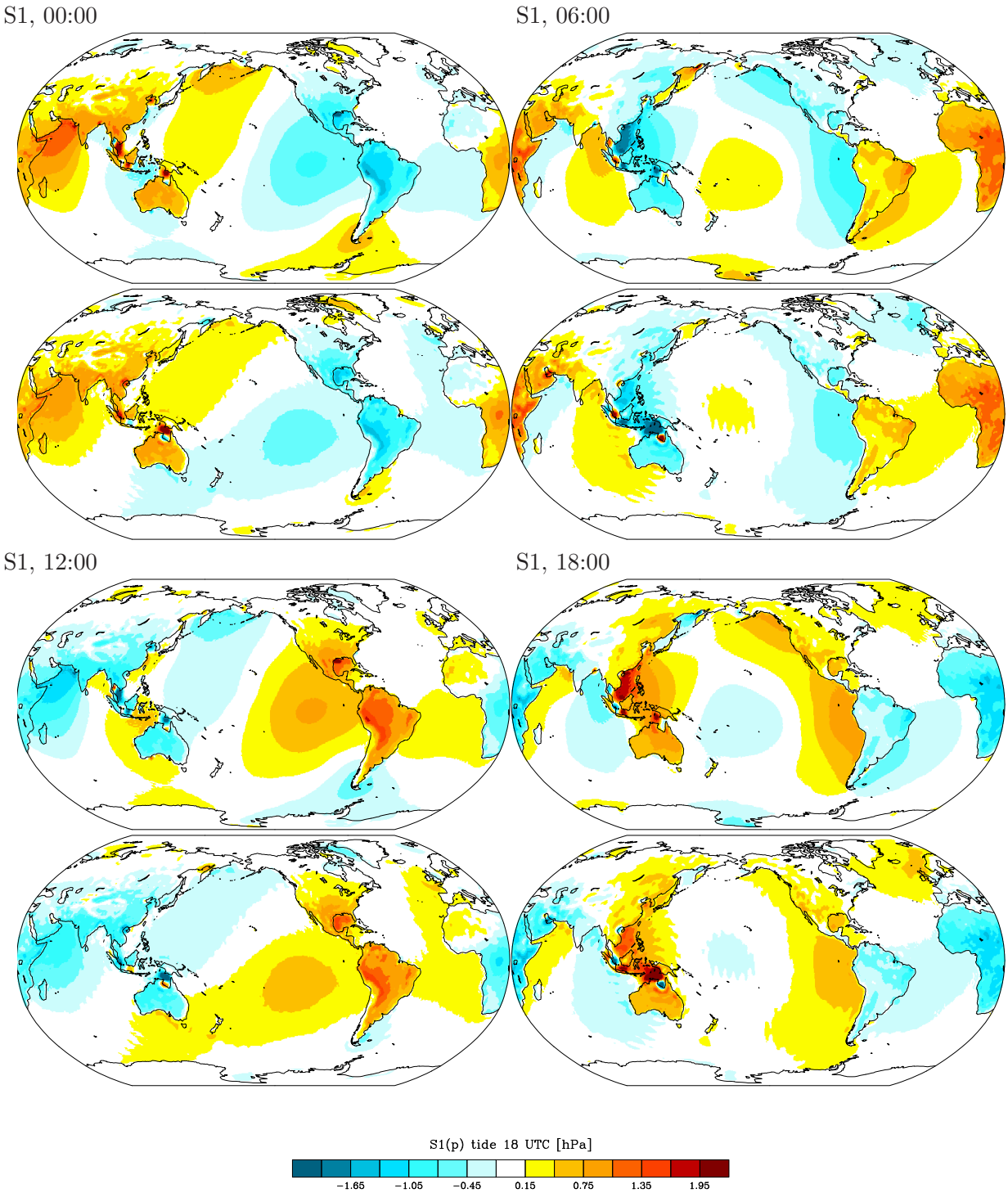

Figure 10.1: Characteristics of the mean atmospheric tide S1(p) and its corresponding oceanic response at 00:00, 06:00, 12:00, and 18:00 UTC as included in the sum of the components A and O from original (first) and updated ESM (second row) averaged over 1995 - 2006.

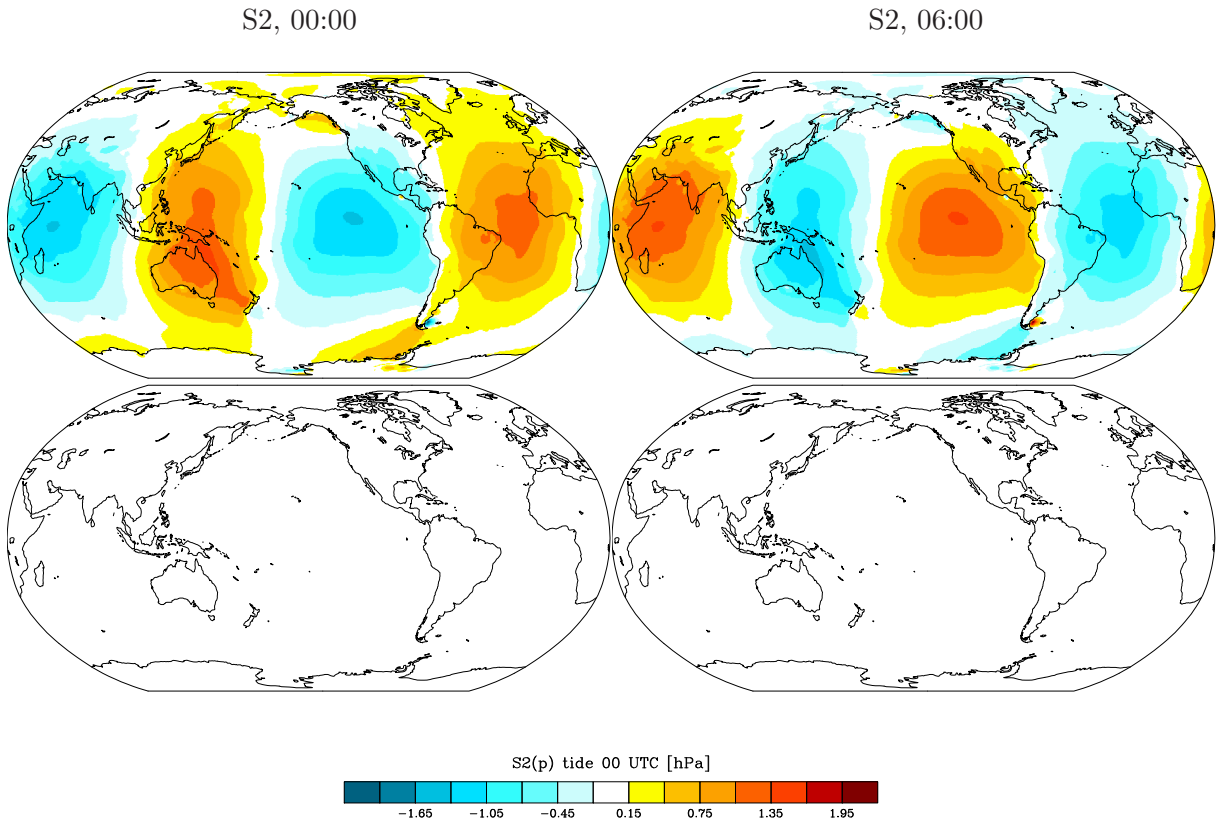

Figure 10.2: Characteristics of the mean atmospheric tide S2(p) and its corresponding oceanic response at 00:00, 06:00 as included in the sum of the components A and O from original (first) and updated ESM (second row) averaged over 1995 - 2006. Note that the updated E SA ESM does not include a mean S2(p) signal.

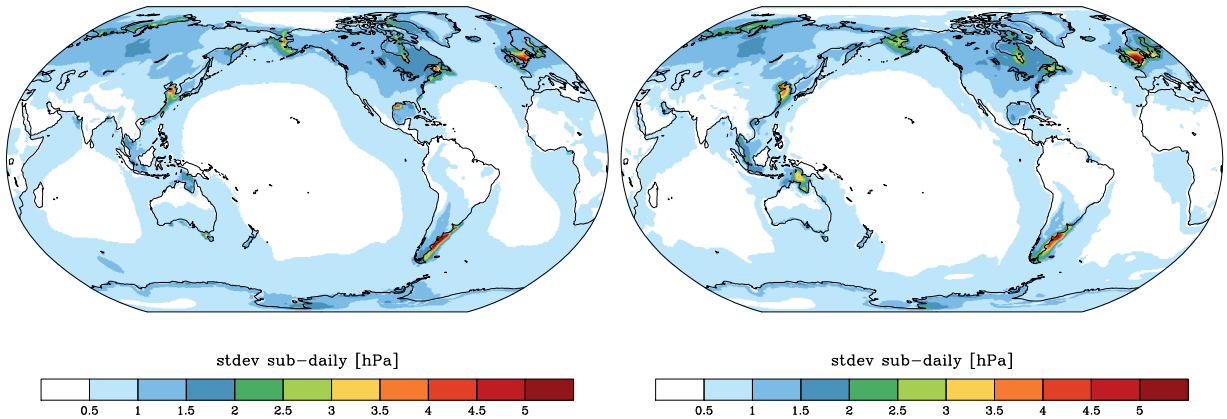

Figure 10.3: Standard deviation at periods between 6 and 24 hours of atmospheric surface and ocean-bottom pressure anomaly (1995-2006) at 0.5^o spatial resolution obtained from the re-synthetized and locally detrended coefficients of the AO component from the original (left) and updated ESM (right).

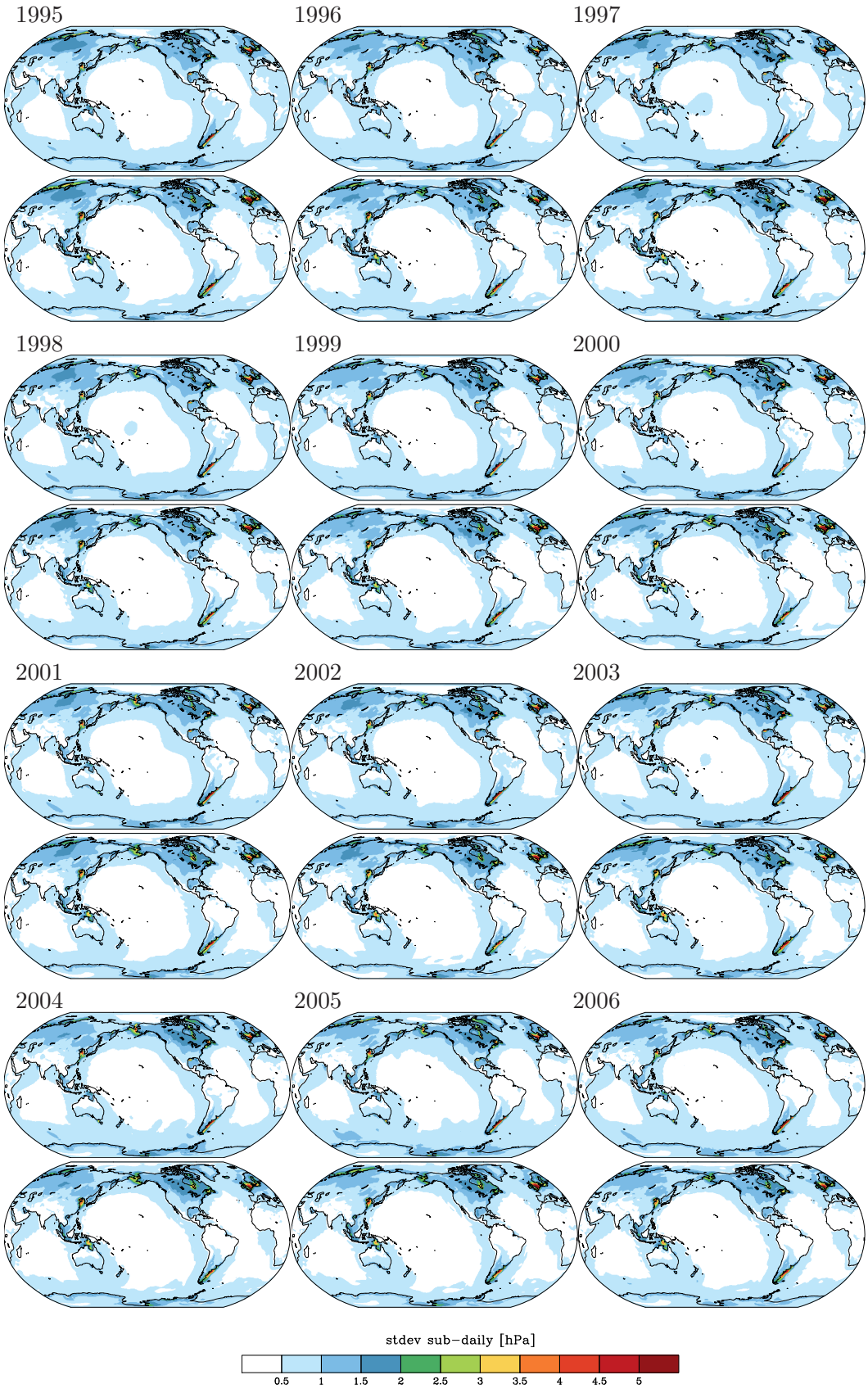

Figure 10.4: Standard deviation at periods between 6 and 24 hours of atmospheric and ocean-bottom pressure anomaly at 0.5° spatial resolution obtained from the re-synthesized, locally detrended coefficients of the AO component from original (first) and updated ESM (second row) for each year between 1995 and 2006.

Bibliography

Bergmann-Wolf, I., Dill, R., Forootan, E., Klemann, V., Kusche, J., Sasgen, I. & Dobslaw, H. (2014). *Updating ESA's Earth System Model for Gravity Mission Simulation Studies, 2. Comparison with the Original Model*, *STR 14/08*, GFZ Potsdam, Potsdam, doi:10.2312/GFZ.b103-14088. 3

Dobslaw, H., Bergmann-Wolf, I., Dill, R., Forootan, E., Klemann, V., Kusche, J. & Sasgen, I. (2014). *Updating ESA's Earth System Model for Gravity Mission Simulation Studies, 1. Model Description and Validation*, *STR 14/07*, GFZ Potsdam, Potsdam, doi:10.2312/GFZ.b103-14079. 3

Forootan, E., Bergmann-Wolf, I., Kusche, J. & Dobslaw, H. (2014). *Updating ESA's Earth System Model for Gravity Mission Simulation Studies, 3. Towards a Realistic De-Aliasing Model*, *STR 14/09*, GFZ Potsdam, Potsdam, doi:10.2312/GFZ.b103-14091. 3

Gruber, T., Bamber, J. L., Bierkens, M. F. P., Dobslaw, H., Murböck, M., Thomas, M., van Beek, L. P. H., van Dam, T., Vermeersen, L. L. a. & Visser, P. N. a. M. (2011). Simulation of the time-variable gravity field by means of coupled geophysical models, *Earth System Science Data*, **3**, 19–35, doi:10.5194/essd-3-19-2011. 3, 11, 13, 49

Klemann, V. & Martinec, Z. (2011). Contribution of glacial-isostatic adjustment to the geocenter motion, *Tectonophysics*, **511**, 99–108, doi:10.1016/j.tecto.2009.08.031. 45

ISSN 1610-0956